Universidade de Aveiro Departamento de Engenharia Mecânica
Ano 2013

Cláudia Sofia de Andrade Redondo Murilhas Buchheim

Comportamento mecânico de AlSiC nanocompositos produzido em moínho de bolas e compactado por *Spark Plasma Sintering*

Mechanical Behavior of AlSiC nano composites produced by Ball Milling and Spark Plasma Sintering

Universidade de Aveiro
Ano 2013

Departamento de Engenharia Mecânica

Cláudia Sofia de Andrade Redondo Murilhas Buchheim

Comportamento mecânico de AlSiC nanocompositos produzido em moínho de bolas e compactado por *Spark Plasma Sintering*

Mechanical Behavior of AlSiC nano composites produced by Ball Milling and Spark Plasma Sintering

Tese apresentada à Universidade de Aveiro para cumprimento dos requisitos necessários à obtenção do grau de Doutor em Engenharia Mecânica, realizada sob a orientação científica do Doutor José Joaquim de Almeida Grácio, Professor Catedrático do Departamento de Engenharia Mecânica da Universidade de Aveiro e coorientação do Doutor Wilfried Georg Smarsly, Diretor de Investigação na Indústria Aeroespacial na Alemanha

Dedico este trabalho aos meus pais, ao meu marido e às minhas filhas, Marie e Sofia.

o júri

presidente

Doutor Helmuth Robert Malonek
Professor Catedrático da Universidade de Aveiro

Doutor Hamid Garmestani
Professor Catedrático do Instituto de Tecnologia da Geórgia

Doutor Saïd Ahzi
Professor Catedrático da Universidade de Estrasburgo

Doutor José Joaquim de Almeida Grácio
Professor Catedrático da Universidade de Aveiro (orientador)

Doutora Maria Leopoldina Mendes Ribeiro de Sousa Alves
Professora Coordenadora do Instituto Politécnico de Leiria

Doutor José Manuel Ferreira Duarte
Professor Auxiliar da Universidade do Porto

Doutora Gabriela Tamara Vincze
Professora Auxiliar Convidada da Universidade de Aveiro

Doutor Wilfried Georg Smarsly
Diretor de Investigacão na Indústria Aeroespacial na Alemanha (coorientador)

agradecimentos

Gostaria de expressar os meus sinceros agradecimentos a todas as pessoas e instituicões que proporcionaram a realização deste trabalho.

Manifesto o meu especial agradecimento ao Professor Doutor José Joaquim de Almeida Grácio por todo o apoio científico, incentivo e permanente disponibilidade.

Um especial agradecimento é dedicado ao Doutor Wilfried Smarsly, que me acompanhou, incentivou e aconselhou na realização desta investigação.

Agradeço ao Doutor Thomas Schubert, IFAM Dresden, pela colaboração na elaboração dos nano compósitos e utilização da técnica " Spark Plasma Sintering", à Doutora Gabriela Vincze pela colaboração na realização dos ensaios mecânicos, aos Doutores Barros Lopes e Lukasz Ciupinski, pela colaboração nas observações por microscopia eletrónica de transmissão e ao Doutor Catalin Picu pela preciosa cooperação na análise e discussão de resultados.

Gostaria de agradecer também ao Senhor Pedro Lima dos Serviços de Gestão Academica, assim como à Doutora Tânia Barbosa da Secretaria do Departamento de Engenharia Mecânica pelo apoio na resolução dos assuntos administrativos.

Manifesto especial gratidão aos meus pais a disponibilidade e ternura com que me acompanharam, ao meu marido, Thorsten, e às minhas filhas, Marie e Sofia.

Finalmente, um agradecimento a todos aqueles que directa ou indirectamente contribuiram para a concretização do meu trabalho de doutoramento.

palavras - chave

Matrix de Aluminio SiC Nanoparticulas Compositos, Mechanismos de Encruamento, Relacão de Hall-Petch.

resumo

Neste trabalho foram produzidos nano-compósitos de Al-SiC misturando alumínio puro com nano partículas de SiC com diâmetro de 45 – 55 nm, usando, de forma sequencial, a técnica da metalurgia do pó e a compactação por " *Spark Plasma Sintering*". O compósito obtido apresentava grãos com 100 nm de diâmetro, encontrando-se as partículas de SiC localizadas, principalmente, nas fronteiras de grão. O nano-compósito sob a forma de provetes cilíndricos foi submetido a testes de compressão uniaxial e a testes de nano-indentação para analisar a influência das nanopartículas de SiC, da fração volúmica de ácido esteárico e do tempo de moagem, nas propriedades mecânicas do material. Para efeitos de comparação, utilizou-se o comportamento mecânico do Al puro processado em condições similares e da liga de alumínio AA1050-O. A tensão limite de elasticidade do nano-compósito com 1% Vol./Vol. de SiC é dez vezes superior à do AA1050. O refinamento de grão à escala nano constitui o principal mecanismo de aumento de resistência mecânica. Na realidade, o Al nanocristalino sem reforço de partículas de SiC, apresenta uma tensão limite de elasticidade sete vezes superior à da liga AA1050-O. A adição de 0,5 % Vol./Vol. e de 1 % Vol./Vol. de SiC conduzem, respetivamente, ao aumento da tensão limite de elasticidade em 47 % e 50%. O aumento do tempo de moagem e a adição de ácido esteárico ao pó durante a moagem conduzem apenas a um pequeno aumento da tensão de escoamento. A dureza do material medida através de testes de nanoindentação confirmaram os dados anteriores. A estabilidade das microestruturas do alumínio puro e do nanocompósito Al- SiC, foi testada através de recozimento de restauração realizado às temperaturas de 150 °C e 250 °C durante 2 horas. Aparentemente, o tratamento térmico não influenciou as propriedades mecânicas dos materiais, excepto do nanocompósito com 1 % Vol./Vol. de SiC restaurado à temperatura de 250 °C, para o qual se observou uma redução da tensão limite de elasticidade na ordem dos 13 %. No alumínio nanocristalino, a tensão de escoamento é controlada pelo efeito de Hall-Petch. As partículas de SiC, são segregadas pelas fronteiras do grão e não contribuem para o aumento de resistência mecânica segundo o mecanismo de Orowan. Alternativamente, as nano-partículas de SiC constituem um reforço das fronteiras do grão, impedindo o seu escorregamento e estabilizando a nanoestrutura. Deste modo, as propriedades mecânicas do alumínio nanocristalino e do nanocompósito de Al-SiC poderão estar relacionadas com a facilidade ou dificuldade do escorregamento das fronteiras de grão, embora não seja apresentada prova explícita deste mecanismo à temperatura ambiente.

keywords

Aluminum Matrix SiC Nanoparticle Composite, Strengthening Mechanisms, Hall-Petch Relationship.

abstract

AlSiC nano composites were prepared by mixing pure Al and 50 nm diameter SiC nanoparticles using a powder metallurgy technique, followed by compression and spark plasma sintering. The final composites had grains of approximately 100 nm dimensions, with SiC particles located mostly at grain boundaries. The samples were tested in uniaxial compression and by nanoindentation in order to establish the effect of the SiC and stearic acid volume fraction, and the milling time on the mechanical properties. The results are compared with those obtained for pure Al processed under similar conditions and for AA1050 aluminum. The yield stress of the nano composite with 1 Vol. % SiC is more than ten times larger than that of AA1050. The largest increase is due to grain size reduction; nanocrystalline Al without SiC and processed by the same method has a yield stress 7 times larger than AA1050. Adding 0.5 Vol. % SiC increases the yield stress by an additional 47 %, while the addition of 1 Vol. % SiC leads to 50 % increase relative to the nanocrystalline Al without SiC. Increasing the milling time and adding stearic acid to the powder during milling lead to relatively small increases of the flow stress. The hardness measured in nanoindentation experiments confirms these trends, although the numerical values of the gains are different. The stability of the microstructure was tested by annealing samples to 150 ºC and 250 ºC for 2 h, in separate experiments. The heat treatment had no effect on the mechanical properties of all samples, except when treating the material with 1 Vol. % SiC at 250 ºC, which led to a reduction of the yield stress by 13 %. In nanocrystalline Al, the flow stress is controlled by the Hall-Petch effect. As observed in this work, the added SiC particles segregate at grain boundaries and do not contribute to strengthening through the Orowan mechanism, rather pin the grain boundaries helping to stabilize the nanostructure of the material. Grain boundary sliding is expected to be important in both nanocrystalline Al and Al-SiC, although we do not present explicit proof for the operation of this mechanism at room temperature.

Table of contents

Table of contents

1. Introduction

1.1 Application of Aluminum Alloys

Aluminum alloys with its remarkable combination of mechanical and physical properties make it the preferred choice as structural material for a wide range of applications in the aerospace, automotive, passenger railway and military industry. Increased market demand for crash and impact resistant light weight structures is nowadays growing also due to the emerging need to protect transport systems against terrorism.

Aluminum is applied for aircraft body structural design. The airframe of a typical current commercial transport aircraft is 80 percent aluminum by weight. Aircraft manufacturers use high-strength alloys, e.g. alloys series 7075 (see Appendix 7.4), with high ultimate strength, and optimized machinability [1].

The European automotive industry, in close co-operation with the European aluminum industry, has developed and introduced numerous innovative light-weight solutions based on aluminum alloys in order to reduce CO_2 emissions. In general a 100 kg reduction of the mass of a car is equivalent to a reduction of 9 grams of CO_2 per kilometer. Aluminum is easy to recycle and saves 95 % of the energy necessary to produce primary aluminum. Industry is working on reducing the cost of other aluminum applications, in particular in the body structure and for chassis and suspension parts, presently used in sports and luxury cars, so that they can also find their place in smaller cars. As a long term vision, an “aluminum-maximized” small family car could be 30-35 % lighter after primary and maximum secondary weight savings [2].

Aluminum made considerable progress in passenger railway cars, where, from trams to trains, many aluminum components were introduced, like window frames and interior partition walls. For the high speed trains, the choice of aluminum proved to be almost a must, as these trains needed to travel at more than 300 km/h on traditional railway tracks. A good example of aluminum's benefits in the public rail transport sector is the TGV-Duplex, developed by Alstom by order of the SNCF, it weighs 12 % less than the traditional TGV, transports 40 % more passengers, and offers superior passive safety.

Also in the military sector there is the growing necessity to improve the aluminum alloys properties to ensure maximum ballistic protection against high velocity projectiles. The 5xxx series strain-harden able alloys have been used in all aluminum military vehicles produced to date. The 7xxx series heat treatable alloys provide improved protection at all angles. Because minimum weight for a given level of protection is essential to mobility, aluminum armor, is used extensively in combat vehicles. The ultimate selection of armor material depends also on requirements other than ballistic criteria, like weld ability, water tightness, machinability, formability and extreme conditions of temperature (-62 to 74 °C), movements through corrosive waters. Strength must be adequate to resist service stresses, including shocks encountered in airdrops and cross-country operation [3].

Additional advantages by aluminum over steel are freedom from low-temperature embrittlement and greater rigidity, resulting from thicker sections, for equal protection. Increased rigidity, up to nine times that of steel, usually eliminates the need for secondary structural support. Production forms of aluminum alloy armor are rolled plate, extrusions, and forgings. For alloys with ballistic properties developed by strain hardening, use primarily is in the form of rolled plate. Heat treatable

aluminum alloys that can be welded effectively are being developed as weld able armor, making it possible to employ more forged and extruded armor components [4].

In summary aluminum alloys are attractive due to their low density, their capability to be strengthened by precipitation, their good corrosion resistance, high thermal and electrical conductivity, and their high damping capacity. The necessity of improving toughness, increased resistance to fatigue and corrosion resistance is driving the future development of advanced aluminum alloys.

One promising approach is to reinforce the aluminum alloy matrix by particles. Aluminum matrix composites are very attractive for their isotropic mechanical properties that are higher than their not reinforced alloys. Aluminum matrix composites offer a large variety of mechanical properties depending on the chemical composition of the aluminum matrix. They are usually reinforced by Al_2O_3, SiC, C, but SiO_2, B, BN, B_4C, AlN may also be considered. The aluminum matrices are in general Al-Si, Al-Cu, 2xxx or 6xxx series alloys. A successful development of aluminum matrix composites is used for brake rotors for German high speed train ICE-1 and ICE-2 developed by Knorr Bremse AG and made from a particulate reinforced aluminum alloy (AlSi7Mg+SiC particulates) supplied by Duralcan. Compared to conventional parts made out of cast iron with 120 kg / piece, the 76 kg of the aluminum matrix composites rotor offers an attractive weight saving potential.

Aluminum matrix composites now used either in sporting goods, electronic packaging, armors and automotive industries [5].

1.2 Motivation

The development of metal matrix composites has attracted attention over the last decades for the purpose of improving fatigue behavior, and strength and creep response as well as impact resistance. Aluminum matrix nano composites are a newer addition to the list of studied materials. These are usually mixtures of ceramic or carbide nanoparticles into an alloy base. The particles are supposed to act as obstacles to dislocation motion and to effectively pin grain boundaries, conferring therefore microstructural stability to the composite. The fillers have very good thermal stability as their melting point is usually much higher than that of the matrix. The matrix may have regular grains of micron of larger dimensions, or nanograins. In the second case, the large density of grain boundaries contributes to strengthening.

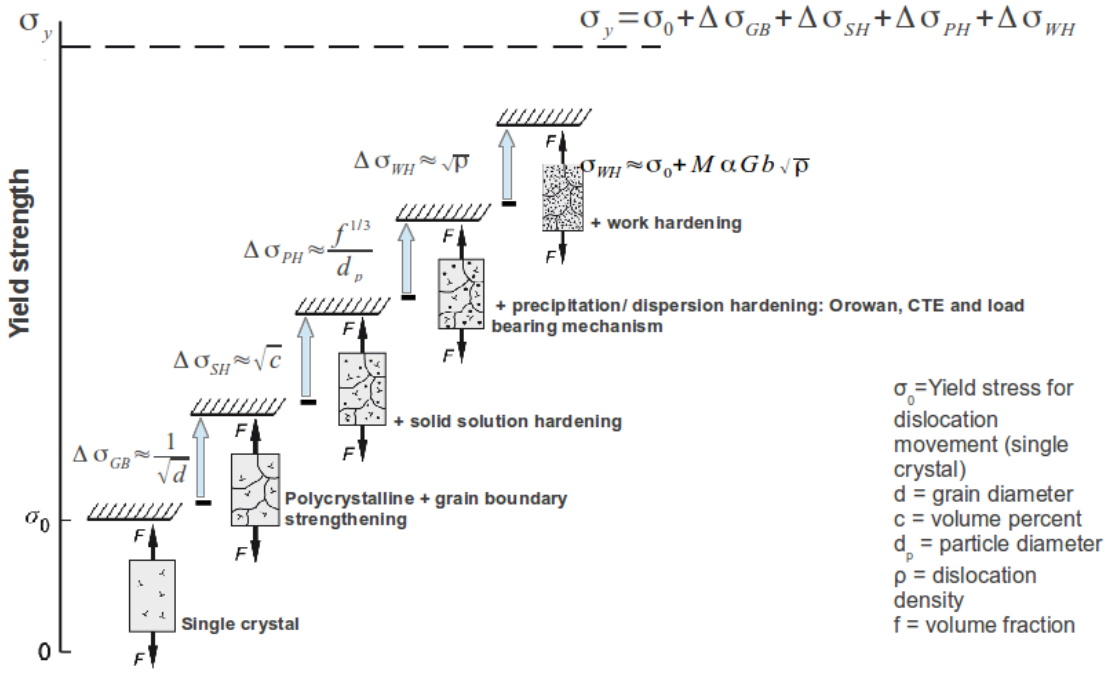

Figure 1: Strengthening mechanism model

The motivation for the thesis is to enhance the mechanical properties of applying the metal physical strengthening mechanism in order to increase the resistance to mechanical loads for aluminum, see Figure 1.

1.3 Objective

The objective of the thesis is the investigation of the strengthening effect of the dispersion of nano-SiC particles in pure aluminum, produced by ball milling of the powders and consolidation by Spark Plasma Sintering (SPS).

In the present work the aim goal is to produce reinforced aluminum composites with SiC nanoparticles by using a powder metallurgy method, which have been studied to achieve a homogeneous dispersion without agglomerations or clustering within a minimum equivalent distance of the reinforced particles in the matrix, believing that such a reinforced material has a high-energy absorption capability and durability. Based on this the presented dissertation includes a manufacturing material composites, defining main parameters as milling methods, milling time, influenced by additional reaction elements, to achieve a multiscale behavior composite material. Experiments made with ball milled material compacted by Spark Plasma Sintering. Analytical methods have been applied for more understanding of strengthening mechanism. The need of utilization of reinforced aluminum with silicon carbide composites in different structural applications has motivated to find a cost effective technological production method for these composites. These composites are characterized for having an enormous complexity in kind of homogeneity, manufacturing and interfacial reaction of the constituents.

1.4 Approach of the thesis

Aluminum matrix nano composites are produced by milling SiC

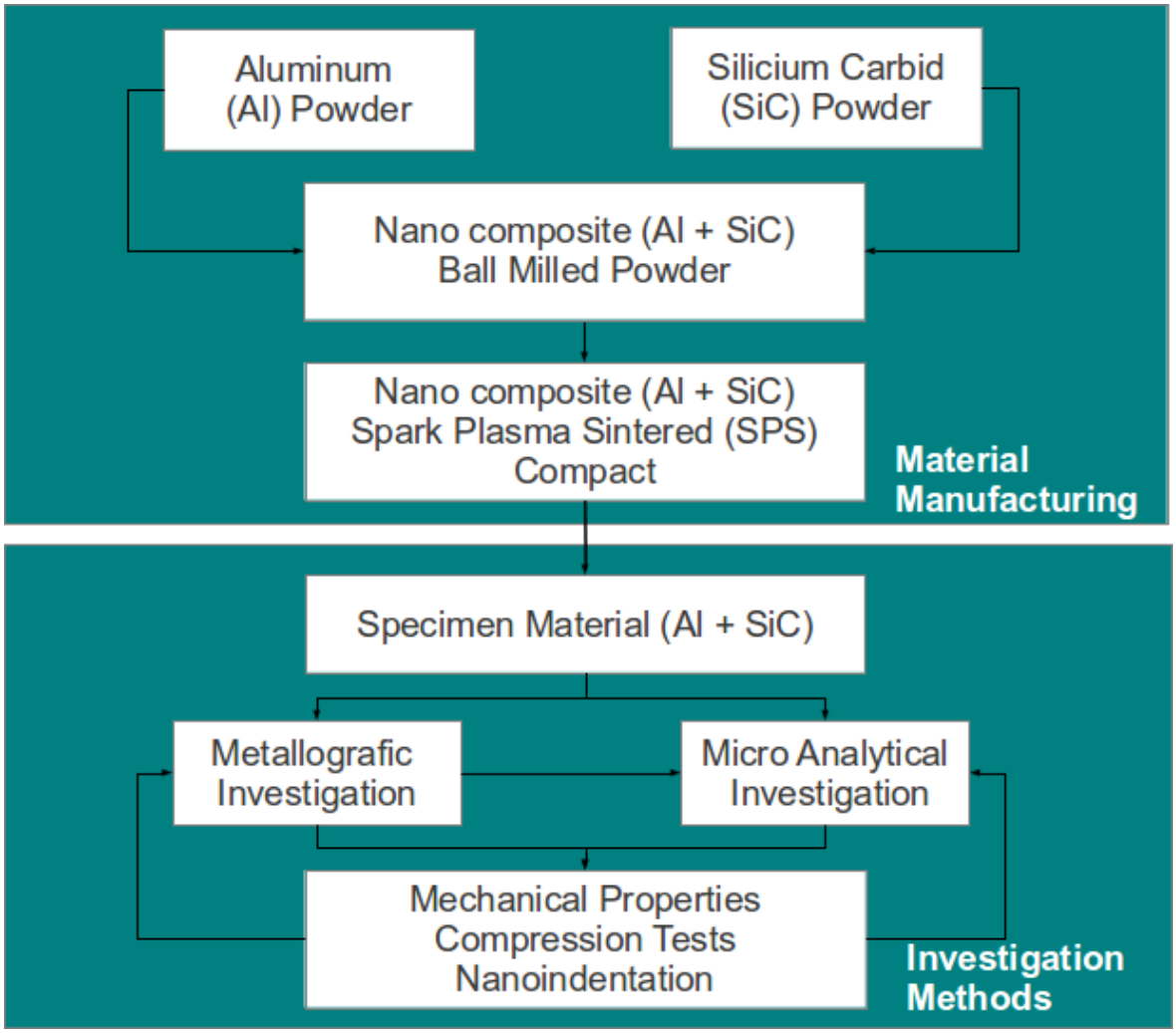

Figure 2: Workflow for the approach of the thesis

nanoparticles into a pure aluminum matrix. A homogeneous dispersion of the reinforcement particles in the matrix should be achieved. To realize this, a powder metallurgy technique involving high-energy ball milling was applied. The milled power was compacted by Spark Plasma Sintering (SPS). The mechanical behavior of the nano composites is probed by performing uniaxial compression and nanoindentation, see workflow in Figure 2.

2. State of the Art

2.1 Strengthening Mechanisms

Nano composites containing nanoscale reinforcement particles have been found considerable attention specially because their superior mechanical properties and higher thermal stability [6], [7], [8], [9]. Although in precipitation hardened alloys nanoscale dispersoids interact with mobile dislocations at room temperature, they suffer from low thermal stability. As a result, precipitate coarsening and dissolving at high temperatures deteriorate the mechanical properties at high temperatures [10].

It is generally recognized that two types of strengthening may occur in metal matrix composites: direct and indirect. Direct strengthening results from load transfer from the metal matrix to the reinforcement particles, whereas indirect strengthening results from the influence of reinforcement on matrix microstructure or deformation mode [11]. For instance, the increase in the dislocation density in the composite matrix due to the mismatch between coefficient of thermal expansion of metal matrix and ceramic reinforcement is assumed to enhance yield strength. However, when the size of ceramic particles goes down to nanometer range there are many doubts about operation of different mechanisms [12], [13], [14], [15], [16], [17].

2.1.1 Load-bearing effect

It is well known that the microstructure and properties of the composite matrix may be significantly different from those of the unreinforced matrix alloy. The presence of hard particles induces an inhomogeneous

deformation pattern even if the composite is subjected to uniform loading. Additionally, higher dislocation density in the composite matrix is assumed to be mainly due to the elastic modulus mismatch.

The idea of the addition of a non-deformable hard phase to a soft metal matrix derives from the load bearing by the second phase with higher elastic modulus. Considering a modified shear lag model (continuum mechanics approach) the contribution of load bearing effect on yield strength is ~ 0.5 V_f (V_f = volume fraction of the second phase) [18]. There is a critical volume fraction below which not only no strengthening would be achieved but also the second phase acts as a defect leading to weakening of the material. Therefore, it is common practice to add a high volume fraction (> 10 %) of the second phase to metals as the reinforcement. However, when the nanoparticles are used as the reinforcement, a much lower amount (< 5 %) is added [19], [20]. Accordingly, the increase in yield strength of pure Al, for instance, with yield strength of σ_{ys} ~ 70 MPa due to load bearing effect of 5 Vol. % of the nanoparticles would be about 1.75 MPa which is negligible.

2.1.2 Orowan Strengthening

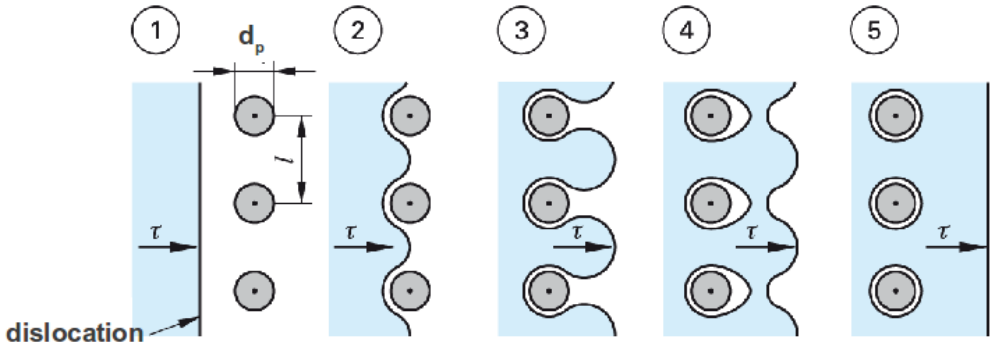

Figure 3: Orowan mechanism for dispersion hardening (Source: James Matsci, Europa Lehrmittel, Werkstofftechnik Maschinenbau, p. 50)

Due to nanoparticle-dislocation interaction by means of the Orowan bowing mechanism, a significant increase in strength of metal matrix nano composites is expected (Figure 3). However, there are several investigations showing that just “effective nanoparticles” can contribute in Orowan strengthening mechanism [8], [19], [21]. The agglomerated nanoparticles should be excluded in the calculation. Furthermore, since the reinforcement is often found to lie on the grain boundaries of the matrix, it is unclear weather the Orowan mechanism can operate. Kang and Chan [19] used quantitative metallography to determine interparticle spacing of effective nanoparticles. They showed that with this modification the predicted yield strengths became closer to the experimental ones. However, there is still a gap between experimental and calculated results and it is more highlighted at higher volume fractions.

Furthermore, depending on the relative size of nanoparticles to matrix grains, the contribution of nanoparticles in Orowan mechanisms could be changed [22]. When the grain size of the matrix is in the nanometer range most of the nanoparticles would be located at grain boundaries forming triple junctions and most probably do not participate in Orowan mechanism. There are several investigations showing when the amount of nanoparticles exceeds a certain value, depending on the size, Orowan island could be formed in which the mobile dislocations would not interact with individual nanoparticles [23], [24]. It was also reported that Orowan strengthening effect reaches its maximum at a critical particle size below which the breakdown of Orowan strengthening occurs. Zhang and Chen [25] calculated the critical particle size for Mg/Al_2O_3 and Ti/Al_2O_3 nano composites by considering relative contribution of improvement factor of Orowan mechanism with respect to that of dislocation. The critical size of nanoparticles is found to be 5.44 times

the Burger's vector or atomic diameter of the matrix. Considering Burgers vector of Mg (b_{Mg} = 0.32 nm), the critical particle size of Al_2O_3 will be smaller than 2 nm. In conclusion, the contribution of Orowan mechanism in strengthening of metal matrix nano composites strongly depends on the matrix microstructure and the location of nanoparticles.

2.1.3 Thermal expansion mismatch strengthening

Higher dislocation density in the composite matrix is assumed to be also due to the coefficient of thermal expansion (CTE) mismatch between the matrix and the reinforcement.

When the material is quenched from processing temperature to room temperature, resulting in a temperature change, mismatch strain due to different coefficient of thermal expansions of the matrix and ceramic particles will be induced.

In order to accommodate this thermal mismatch deformation, Dai et al. [11] considered that geometrically necessary dislocation loops will be imposed around the surfaces of particles.

The increase in yield strength due to the coefficient of thermal expansion has been calculated and reported as a main strengthening mechanism for different nano composite systems. At a fixed volume fraction as the particle size decreases the number of dislocations around an individual particle decrease, while considering the overall number of nanoparticles the dislocation density is higher rather than those in microcomposites. Zhang and Chen [25] reported for example in Mg/Al_2O_3 system, a remarkable increase in strengthening would be achieved with decreasing the particle size from 1000 to 10 nm. Considering the increased dislocation density due to the CTE mismatch, one can calculate enhancement in yield strength by the Taylor dislocation strengthening relation [11].

Most often, considering average particle size and volume fraction of nanoparticles the increase in yield strength due to the coefficient of thermal expansion has been calculated and reported as a main strengthening mechanism for different nano composite systems.

Accordingly, there is a critical particle size below which strengthening due to CTE mismatch cannot intervene any more. For instance, the critical size of nanoparticles for aforementioned system is as ~30 nm. However experimentally it is not proved if there is any dislocation around nanoparticles as a function of particle size and cooling condition. Very recently, Vogt et al. [26] reported the absence of thermal expansion mismatch strengthening in nanostructured metal–matrix composites.

2.1.4 Grain boundary strengthening

Large increase in strength and hardness is frequently documented for ultrafine structures, a phenomenon that is explained in part by small grain sizes using the well-known Hall-Petch relationship. However, there are many reports showing the occurrence of inverse Hall-Petch phenomena in nanometer range [27], [28], [29], [30]. Grain boundary sliding, Coble creep and triple junction diffusional creep are considered as the main reasons for this phenomenon. Based on the well-known pileup model, Hall-Petch equation, as the grain size decreases the number of dislocations that pile up behind the grain boundaries decreases and consequently stress concentration would be decreased. Under this condition higher stress level is required for initiation of plastic deformation, by dislocation motion. At the other extreme for very small grain sizes, it is assumed that Coble creep is active. However when nanoparticles are added to the matrix, pining course of action suppresses grain boundary sliding and diffusional creep. Higher creep

resistance of super alloys and dispersion strengthened matrices are frequently reported. Formation of smaller grains and suppression of grain growth in oxide dispersion alloys and nano composites are resulted from the pining of grain boundaries by nanoparticles. Kang and Chan [19] reported that in Al/Al_2O_3 nano composites the grain size of the aluminum matrix is decreased by of the addition of nanoparticles. However, the minimum grain size was obtained for Al - 5 Vol. % Al_2O_3 nano composite in which further increase in the amount of nanoparticles did not lead to smaller grain size. Therefore, there is a critical volume fraction dependence on size and type of nanoparticles to pin grain boundaries.

However, different models have been developed to predict the final grain size of the matrix as a function of nanoparticles size and volume fraction. According to the Zener model [31], the grain size of aluminum matrix nano composite containing 5 Vol. % nanoparticles with an average diameter of 50 nm is calculated to be ~ 650 nm. Using Gladman model [32] the minimum grain size in nano composite could be predicted by 338 nm. Free of agglomerates and more homogenous distribution of nanoparticles in mechanically milled nano composite powder resulted in formation of smaller grain size at the end. In terms of energy, Kamrani et al. [33] showed that the grain size of Al – 5 Vol. % SiC nano composite is 173 nm while Kang and Chan [19] reported the grain size of 1.1 µm for Al – 5 Vol. % Al_2O_3 nano composite. The former was fabricated by mechanical milling followed by double press double sintering while the latter was fabricated by mixing/HIP/hot extrusion.

Although, theoretically the final grain size is dictated by the size and volume fraction of nanoparticles the fabrication method significantly affects the final microstructure. Kang and Chan [19] reported that in Al – 5 Vol. % Al_2O_3 grain boundaries are saturated by nanoparticles. A more

precise investigation of microstructure revealed the presence of large agglomerates (100 - 400 nm) reducing the efficiency of nanoparticles in hindering grain growth. Thus, just the addition of nanoparticles does not guarantee the formation of smaller grain size.

When second particles lie at the grain boundary, the interface energy reduces because a part of boundary area is occupied. If this part of the grain boundary moves away from the second particle, the interface energy will increase due to the increase of the grain boundary area. Only if the reduction of the free energy of the system resulting from microstructural evolution exceeds the increased interface energy can the part of grain boundary continue to move, otherwise the part of the grain boundary is pinned by the second particle [34]. As for second particle with larger size, there is stronger interaction between second particle and the grain boundary because the interface energy may be more decreased when the larger second particle occupies part of the grain boundary. However, at a fixed volume fraction, the smaller the second particles size, the larger the number of second particles, and the greater the second particles dissipating degree in the space.

Accordingly one can conclude that there is a critical second particle size with the maximum ‘unpinning’ tendency of grain boundary while the second particle dissipating degree in 3 dimensional space should be considered. However, Durisin et al. [35] showed abnormal grain growth in Cu-3 Vol. % MgO nano composites leading to formation of a structure with a bimodal grain size distribution: micrometre-sized grains embedded inside a matrix of nanocrystalline/ultrafine grains. Due to the weak coherency of Cu – MgO interface, the matrix is not sufficiently controlled by the MgO during heating. MgO agglomeration does not strengthen grain boundaries.

In summary, the grain size of the matrix is directly dependent on the

nanoparticles type, size, volume fraction and distribution. Regarding this fact, to predict the contribution of grain boundary strengthening at higher volume fraction the grain size should be considered smaller. Zhang and Chen [36] did not consider this effect in their model. Moreover, nanoparticles located at grain boundaries cannot interact with mobile dislocations via Orowan mechanism. Very recently, Razavi et al. [37] modified Zener model [31], in nanostructures obtained by evaluating a non-random distribution of incoherent ceramic particles. On the basis of the new analysis, the grain size of aluminum matrix nano composites containing 5 Vol. % nanoparticles with an average diameter of 50 nm would be ~244 nm.

During processing of the nano composite, grain boundary movement leads to decoration of grain boundaries with nanoparticles. Ferkel et al. [8] showed formation of a nanoalumina dispersed zone along grain boundaries in Mg/Al_2O_3 nano composite surrounding alumina depleted zone. Referring to this obtained structure one can conclude that nanoparticles are mobile and can move along grain boundaries at high temperatures. Pinning of grain boundaries by sufficient number of nanoparticles led to termination of grain growth course of action. Srinivasan and Chattopadhyay [38], showed that in ternary aluminum alloys precipitation of nanodispersoids on grain boundaries resulted in a significant increase in the slope of Hall-Petch equation which is referring to an increase in strength caused by the grain boundaries.

Srinivasan et al. [39] reported vastly different Hall-Petch constant values (ky) in nanocrystalline NiCr with nanoscaled Y_2O_3 and Al_2O_3 dispersoids. They attributed this phenomenon to grain boundaries whether are decorated with particles or have any preferential orientation, namely texture. Very recently Cao et al. [40] reported that segregation of Mg solute atoms along grain boundaries of Al resulted to larger ky value.

Seemingly, nanoparticles located on grain boundaries play dual roles: decreasing the grain size and increasing the grain boundary strength (ky) while they cannot contribute to Orowan mechanisms. Probably due to the fact that they are located at grain boundaries, a disordered region in crystalline structure one can conclude that to compensate CTE mismatch between ceramic and metal matrix no geometrically necessary dislocations would be generated at the grain boundaries. As a consequence they will not lead to increase of yield strength by increase in dislocation density. Therefore, strengthening mechanisms should be weighted as a function of effective volume fractions of nanoparticles playing different roles.

To have a better insight on the effect of nanoparticles on grain boundary strength, the slope of Hall-Petch equation, data reported in reference [19] was reanalysed by considering possible strengthening mechanisms. Yield strength of Al/Al_2O_3 nano composite as a function of grain size extracted from reference [19]. As seen, with the increase in the volume fraction of Al_2O_3 nanoparticles, grain size decreases while yield strength increases. In general, yield strength can be predicted by superimposition of different mechanism. Since the maximum volume fraction of Al_2O_3 nanoparticles is < 6 %, this effect is negligible. As specimens have been fully annealed, quench strengthening due to CTE mismatch can be excluded as authors reported before in Reference [19]. If we assume that all nanoparticles are located at grain boundaries will become zero. Under this condition grain boundary strengthening should be the main strengthening mechanism.

As reported in [19], grain boundaries are decorated with nanoparticles. As mentioned before, decorated grain boundaries with nanoparticles exhibit higher ky value in comparison with unreinforced alloy. If one assumes that nanoparticles on grain boundaries just strengthen grain

boundaries, an increase in the slope of Hall-Petch equation should be expected. The slope of Hall-Petch line is 0.178 $MPam^{-0.5}$ which is much higher than 0.07 $MPam^{-0.5}$ for pure Al [19]. The obtained ky value is similar to that in Al2Mg2Li alloy containing Al_3Li precipitates [41]. Since a part of nanoparticles are introduced inside the grains, the effect of Orowan strengthening mechanism should be taken into account. However, the enhancement in ky value decreases and reaches the value for unreinforced aluminum while no particle is located at the grain boundaries.

On the basis of a simple assumption, ky value can be changed in the range of dependent on the location of nanoparticles with respect to grain boundaries. Although, Kang and Chan [19] used quantitative metallography to determine the effective interparticle spacing and calculate more reliable Orowan stress, there is a big gap between experimental and theoretical results. One can use reverse calculation to find interparticle spacing and effective volume fractions of nanoparticles on the basis of experimental results.

Considering grain size and yield strength mentioned above, the effective volume fraction of nanoparticles contributing to Orowan mechanism were calculated and drawn as function of the slope ky. Interestingly, ky for unreinforced Al 0.07 $MPam^{-0.5}$, the calculated effective volume fraction is more than 8 % while the total volume fraction of nano-Al_2O_3 is 4 %. With the increase of ky value, the calculated effective volume fraction decreases and at ky = 0.13 $MPam^{-0.5}$ it reaches to ~2.4 %, which is acceptable. The same trend can be observed for nano composites with different amount of nanoparticles.

2.1.5 Summary of strengthening mechanisms

In the present study, a new perspective is presented to relate the contribution of different strengthening mechanisms as a function of effective volume fraction of nanoparticles. Based on the distribution pattern of nanoparticles and their location with respect to grain boundaries three different nanoparticles were considered: 1) nanoparticles distributed inside the grains, 2) nanoparticles located at grain boundaries or triple junctions and 3) clustered nanoparticles. The first group of nanoparticles can interact with mobile dislocation and strengthen nano composite via Orowan bypassing mechanism, as shown in Figure 3. The second group which is nanoparticles located on grain boundaries pins grain boundaries and enhances grain boundary strengthening by changing the slope of the Hall-Petch equation. Nanoparticle larger than a critical size can contribute in strengthening by CTE mismatch. On the base of dislocation theory, the critical particle size was found the size that smaller than that no geometrically dislocation can be generated around nanoparticles.

2.2 Nano composite manufacturing processes

2.2.1 Melting Technology

It is known that the distribution of hard particles throughout the matrix has a vital influence on the mechanical properties of composite materials [42]. When nanoscaled reinforcements are used, agglomeration and clustering of the particles are critical issues which affect mechanical properties significantly [19]. Ultrasonic dispersion of nanoscaled ceramic particles in molten Al [43] and Mg [44] has been employed to distribute nanoparticles throughout the matrix but no significant increase in mechanical properties was obtained (Figure 4).

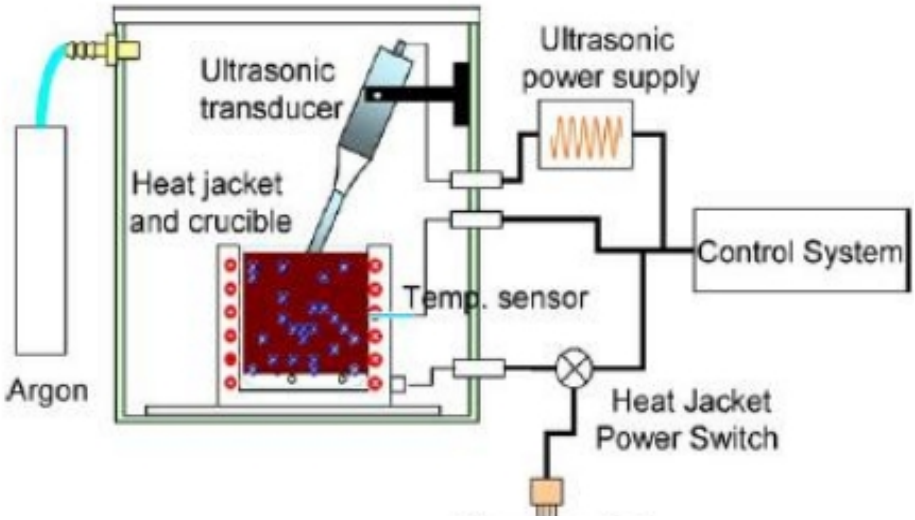

Figure 4: Schematic diagram showing the experimental setup of ultrasonic method (Source: Hao Yu, (2010), Thesis submitted to the Faculty of the Worcester Polytechnic Institut).

The most important challenge is the poor wettability of the particles by the melt [21], [22]. This limits the concentration of fillers that can be properly dispersed to approximately 4 % [23]. In addition, due to the high temperature of the melt, chemical reactions take place at the interface between fillers and the matrix, leading to the formation of a brittle interphase whose presence reduces the material performance. An investigation on the structure of an ultrasonically cast nano composite of Al with 2 Wt. % nano-sized Al_2O_3 dispersoids showed that the nano composite consisted of nearly continuous nanoalumina dispersed zones in the vicinity of the grain boundaries encapsulating Al_2O_3 depleted zones [6].

Production methods like casting have these advantages of problems of

reinforcement segregation and clustering, interfacial chemical reactions, high localized residual porosity and poor interfacial bonding. Other production methods such as spray deposition are not applicable because of it expensive costs.

2.2.2 Powder Metallurgy

Powder metallurgy technique such as mechanical milling is another

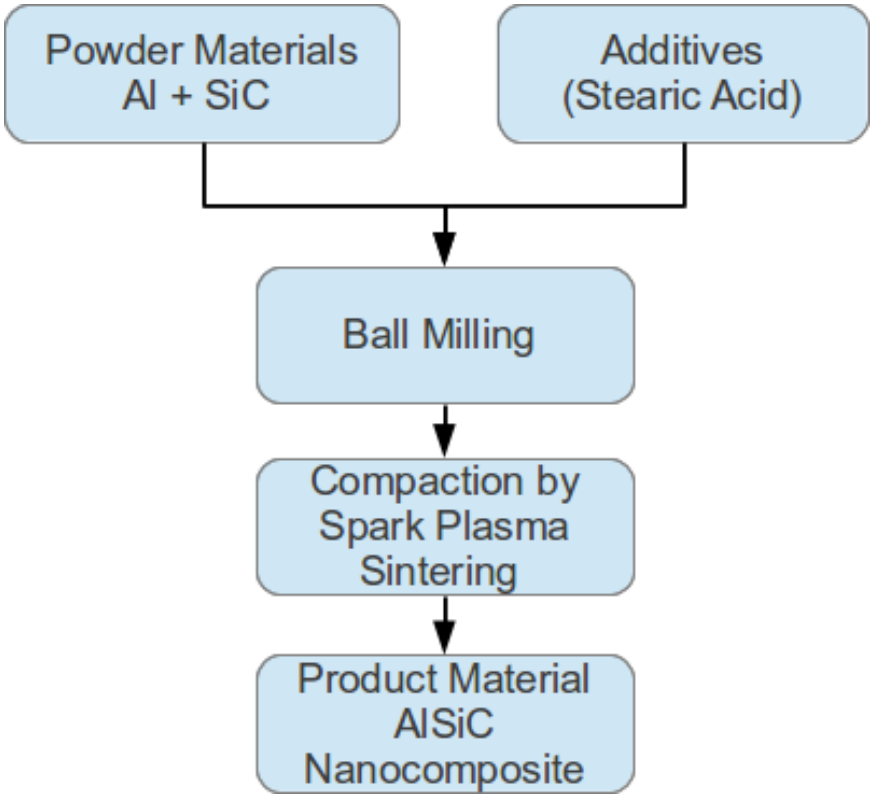

Figure 5: Conventional powder metallurgy process

procedure to distribute nanoparticles throughout metal matrix. A conventional powder process is shown in Figure 5. Naser et al. [6] have shown that this method is a novel approach for dispersion strengthening of metals by nanoparticles. Tang et al. [45] reported a relatively homogenous distribution of SiC nanoparticles in Al-5083, see Appendix

7.4, matrix by the milling process.

Although mechanical milling helps to distribute nanoparticles throughout the matrix, structural investigations show formation of decorated grain boundaries. For instance, Ferkel and Mordike [9] showed that in the case of hot extruded milled powders a sub micrometer grained Mg structure was developed with the nanoscaled SiC particles decorating the shear band near grain boundaries.

The most promising industrialized fabrication technology is powder metallurgy-based [9], [10], [42]. This method requires mixing the two materials in the powder form, mechanical alloying by ball milling, followed by pressing, sintering and/or hot processing like extrusion.

This method allows avoiding issues with miscibility and generally leads to sharp, mechanically strong interfaces between nanoparticles and matrix. An important drawback of the method is the fact that samples are porous and achieving full density requires increasing the temperature, i.e. performing a hot processing step. This leads to some grain growth, although enhanced stability of the composite microstructure to microstructural coarsening has been reported [19], [43].

It is interesting to note that compaction of powder containing grains of nanometer dimensions, and especially when ceramic or carbide nanoparticles are incorporated, is more difficult than the compaction of micron-sized powder of the same metal or alloy [44], [45]. This is because plasticity in nanocrystalline samples requires order of magnitude larger stresses and spring back is more pronounced. Therefore, nanostructured samples are likely to be more porous. Milling is also affected by the presence of nanoparticles [44], [45].

During this operation, the initial particles are welded together and fractured repeatedly. The powder size in a milling operation may

increase initially, before decreasing. A steady state results when the welding and fracturing rates become equal. Powder particles become equiaxed when this regime is reached. If hard nanoparticles are present, the rate of milling increases and the steady state regime is reached faster. This is attributed to the stress concentration effect of particles and their contribution to dislocation nucleation and plastic deformation.

Milling leads to uniform distribution of fillers and induces a strong grain size reduction, both effects being beneficial to strength properties. Powder metallurgy has the advantage of producing net-shape components minimizing machining process which is a great problem in case of aluminum silicon carbide composite as a result of high tool wear due to the inherent abrasiveness of the hard SiC particles. Also the machining process causes cracking of SiC particles and debonded matrix-reinforcement underneath the machined surface.

However the aluminum silicon carbide composite produced by powder metallurgy in addition to an acid-stearic increases the strength relatively. The acid-stearic film surrounding the nano-Sic nanoparticles protects it reinforcement and homogeneous distribution and movement of dislocations at the boundary or through them and produces high strength, brittle, and insensitivity to high temperature exposure composite.

In most works to date, aluminum was mixed with either silicon carbide (SiC) [12], [11], [13], [14], [15], [16] or alumina (Al_2O_3) nanoparticles [17]. Filler concentrations up to 20 % have been considered, while the base metal was either pure Al or one of the commercial Al alloys. In most works, the nanoparticles are embedded in a nanocrystalline metal [16], although this is not always the case [13]. Significant increases of the yield and flow stress, and of hardness have been reported for some of these materials [13].

The Spark Plasma Sintering (SPS) is a promising sintering technology to produce dense bulk pre-compacts from micro- or nano-structured aluminum alloys at lower temperatures and shorter sintering times.

Spark Plasma Sintering is one of the most recent techniques [41], [46], [47]. Regardless the controversy to the presence/absence of sparking [48], important technological benefits such as short processing time, fewer processing steps, elimination of the need for sintering aids, and near net shape capability are unchallenged. In addition, the use of high heating rates and short dwell times can minimize grain growth, which often leads to improved material properties. Several experimental studies [49], [50] on the effect of pulsed current sintering on microstructure and mechanical behaviour of pure and alloyed aluminum powders demonstrated the capability of SPS in maintaining a very fine microstructures for a excellent mechanical performance of the bulk material. The breakdown of the oxide layers on the aluminum powder particles is one of the challenges for successful sintering of aluminum.

The available experimental results suggest, the SPS process can promote the elimination of the closed oxide layers and therefore promote the sintering by localised heating at the contact areas in combination with a sufficient pressure on the powder. In addition, the necessary degassing step for aluminum powder should be also feasible in a short time by employing the sintering cycle to remove the adsorbed gas on the particles effectively. But, the measured tensile mechanical properties of aluminum compacts consolidated by SPS scatter between lower and comparable with that of a corresponding wrought or extruded compact [51], [52], [53], [54]. Therefore, it seems, that no comprehensive understanding regarding the influence of the SPS sintering process parameters and material characteristics exists today [55].

3. Experiments

3.1 Manufacturing of Specimen Materials

3.1.1 Powder Materials

The materials used in this work are 99.99 % pure Al powder and 97.5 %

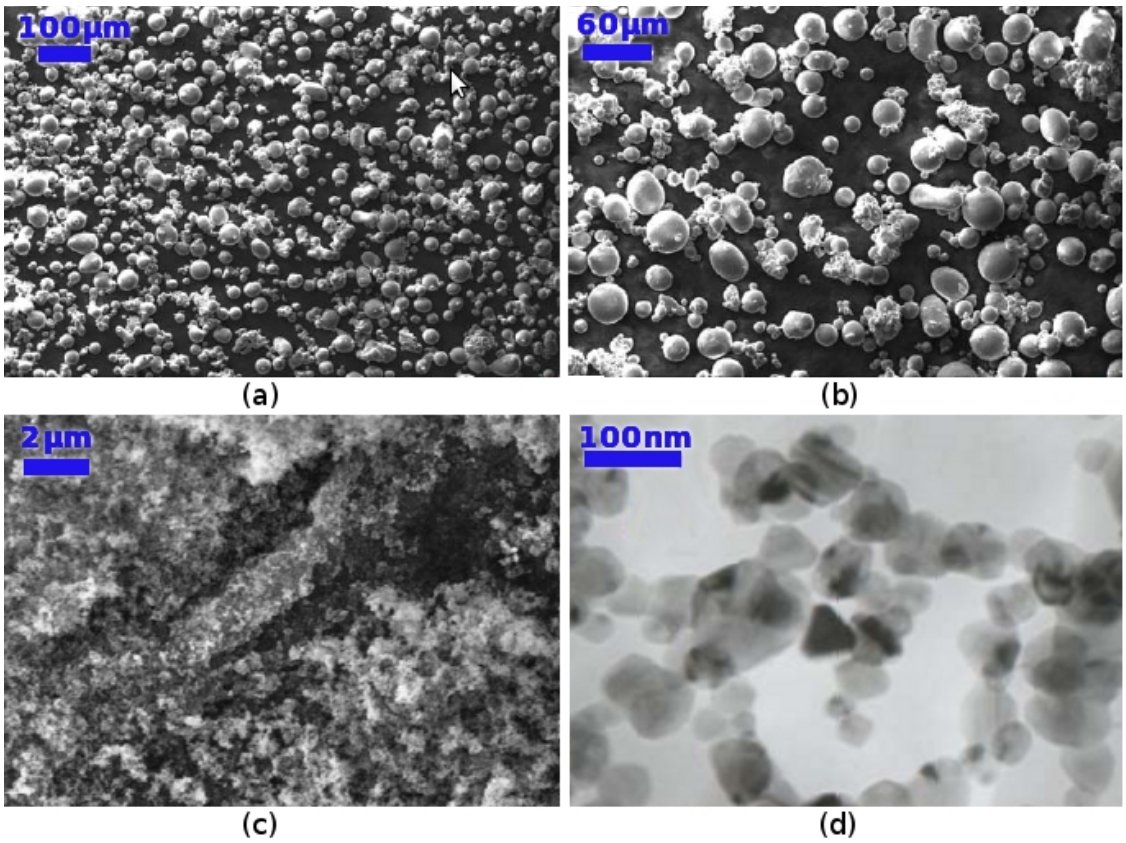

Figure 6: (a) and (b)Al99,99 <50µm of ECKA Granulates, Germany,(c) and (d) beta SiC, 97.5 %, 45-55 nm, NanoAmor, USA,

pure SiC. The Al powder had spherical particles of rather polydisperse diameter < 50 nm. The SiC particles were more facetted than the Al ones and have nominal dimensions of 50 nm, as shown in Figure 6.

3.1.2 Milling Process

The proper amounts of Al and nanoparticles were weighted to prepare Al-xSiC (x= 0 / 0.5 / 1 Vol. %) nano composite mixtures. The powders were blended in a Turbula mixer.

Then, the mixtures were milled in the high-energy planetary ball-mill Pulverisette P5 of Fritsch, Germany (Figure 7).

Figure 7: High energy ball milling with Pulverisette P5 (Fritsch, Germany), steel container (250 ml) filled with 100 balls (100 Cr6, 10mm diameter, 100 balls) stearic acid (0,5 or 1,0 Wt.%) rotation speed varied between 150 and 250 rpm 10 gram powder per milling vessel

Small amounts (0.5 and 1 Wt. %) of stearic acid were added as process control agent (PCA) to prevent detrimental welding effects to the milling containers and balls. The steel ball to powder weight ratio was 10:1. The rotational speed was 250 rpm and milling was performed under a high purity argon atmosphere. The high energy milling time was 4.5 h and 13.5 h for the different materials.

The summary of the milling parameters and Samples is listed in the Table 2, see Appendix 7.5. In order to study the effects of varying milling parameters this work has been realized in three steps. At first the main influencing parameters were analyzed very carefully. Secondly the speed and time of milling were evaluated. Finally the quantity of milling balls and the quantity of PCA as well as the milling time were varied.

3.1.3 Spark Plasma Sintering Process

Cylindrical samples of 8 mm diameter and 10 mm height were consolidated using the Spark Plasma Sintering system HP D 5 of FCT Systeme GmbH, Germany. The Spark Plasma Sintering Process can be understood as a modified hot pressing technique.

Figure 8 shows the equipment where the samples has been consolidated using Spark Plasma Sintering.

The sample is heated by a pulsed electric current (1) which flows through the punch-die-sample-assembly using a high current and low

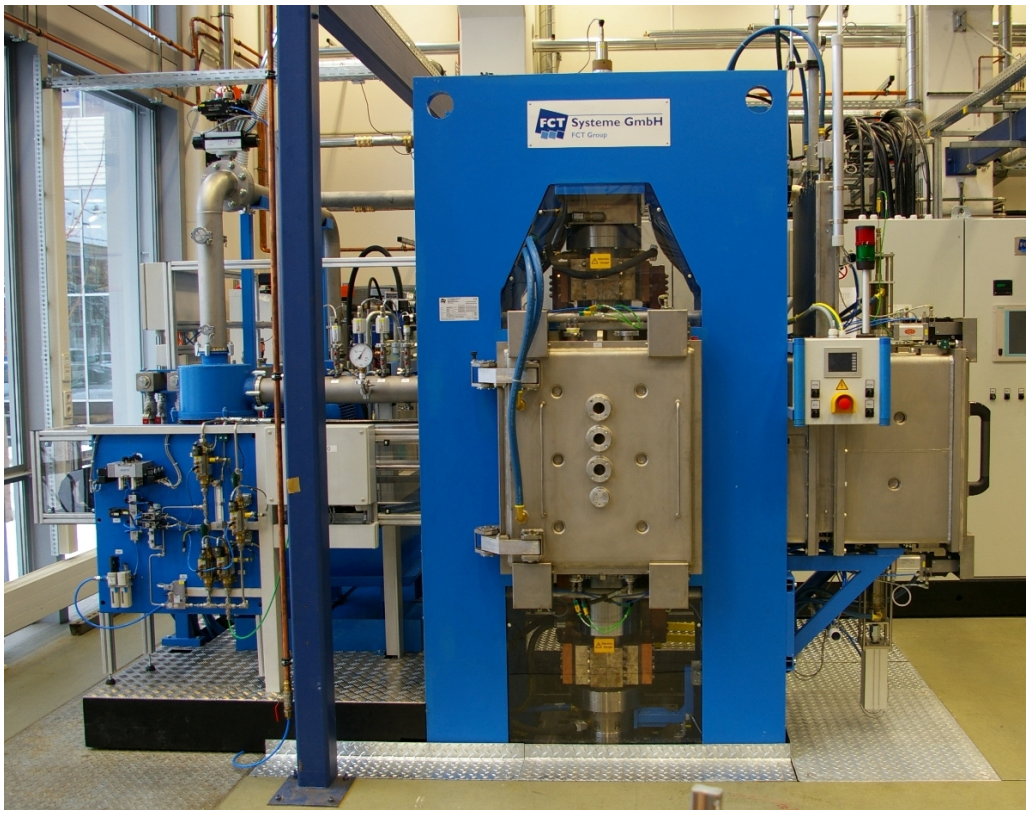

Figure 8: Spark Plasma Sintering system HP D 5 of FCT Systeme GmbH, Ø8 mm steel die, 450 °C/ 5min/ vacuum/200 MPa [IFAM Dresden]

voltage. In contrast to other sintering techniques a special preparation

of the sample, i.e. by cold pressing, is not necessary, because the powder is filled directly in the mold, Figure 9. Six types of materials are discussed in this work and are listed in Table 2, see Appendix 7.5., Material 1 is commercially pure aluminum AA1050, obtained from Alcoa Inc.. This material is not produced by powder metallurgy and has large grains of approximately 200 nm. It is taken as reference in this work.

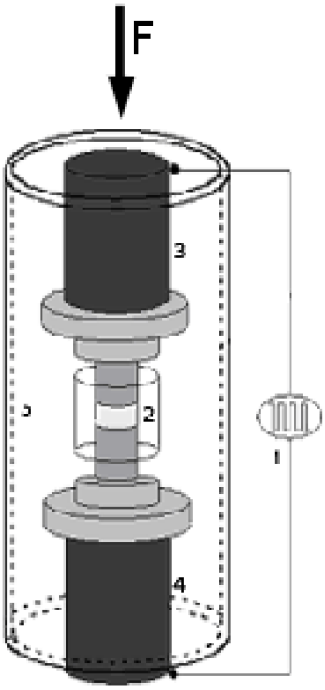

Figure 9: Scheme of a SPS-system: 1- pulsed current generator, 2- pressing tool with sample, with a strength F in one direction, 3- upper punch, 4- lower punch, 5- water-cooled vacuum chamber (Source: IFAM Dresden)

Material 2 does not contain SiC nanoparticles and is obtained by powder metallurgy process following the method described above. The powder was mixed with 1 Wt. % stearic acid and milled for 13.5 h.
Material 3 is processes under similar conditions, except that 1 Vol. % SiC powder was added. Materials 4, 5 and 6 differ from material 3 by the SiC and stearic acid concentration and by the milling time see Appendix 7.5

Table 2.

The overview of SPS materials samples is listed in Table 2, see Appendix 7.5 and Figure 10 shows as example the SPS samples material 5 and 6.

(a)

(b)

Figure 10: SPS materials samples (a) Material 5, (b) Material 6

3.1.4 Annealing Treatment

The microstructural stability of these materials is essential in applications. In aluminum in particular, grain growth at ambient temperature is expected to take place leading to flow stress reduction and ductility improvement. To investigate this issue we selected the material leading to the highest yield stress, material 3, and its equivalent without SiC, material 2, and subjected them to accelerated aging by annealing at 150 ^{o}C and at 250 ^{o}C, in separate experiments, for 2h. The samples were fully characterized by TEM, macroscopic uniaxial testing and nanoindentation after each annealing sequence. The annealed materials 2 are denoted as 2HT150 and 2HT250, while the annealed materials 3 are labeled as 3HT150 and 3HT250.

For all materials studied the density was measured using the gravitational technique by measuring the weight in de-ionized water and 70% isopropyl alcohol. The results of the density measurements are shown in the Appendix 7.5 Table 1.

3.2 Microstructural and Microanalytical Investigations

3.2.1 Metallographic Investigations

Figure 11: Material 4 (a) milled powder particles, (b) metallographic section of milled powder particle, (c) (b) at higher magnification showing impurities (circled)

The surface of the metallographic specimen was prepared by standard grinding, polishing and etching procedures used for aluminum alloys. These investigations were performed at Fraunhofer Institute for Manufacturing and Advanced Materials, IFAM, Dresden. After preparation, the specimens were analyzed by optical and electron microscopy. For optical microscopy a stereo microscope was used.

More or less round balls with millimeter size, without welding, have been obtained (Figure 11). Increasing the PCA, acid stearic from 0,5 Vol. % to 1 Vol. % the size of the milled powder particles is relatively homogeneous. Smaller particles can be observed but with a homogeneous size. In the different cross sections of the powder particles some pores and inclusions were observed.

The results were obviously dependent on the used quantity of the process the process control agent, PCA, stearic acid, there was no sticking of aluminum on the inner wall of the container and the balls.

3.2.2 Scanning Electron Microscopic Investigations

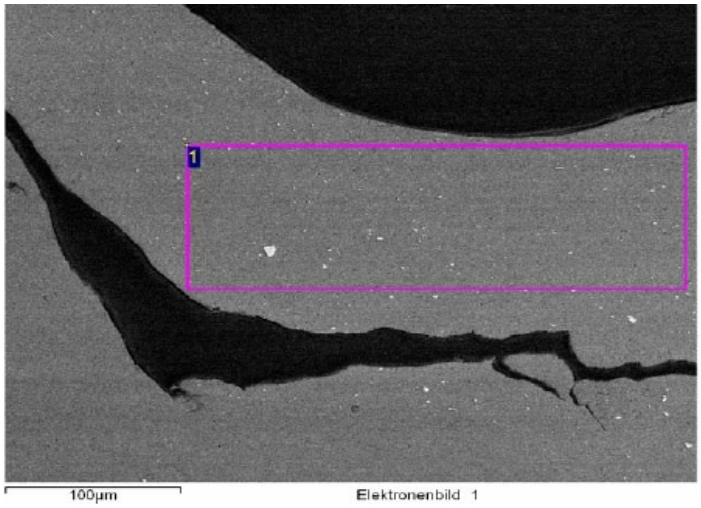

Spektrum	O	F	Al	Si	Ca	Ni	Summe
	in wt.%						
1	2.31	6.09	89.81	0.83	0.30	0.66	100.00

Figure 12: Material 4, EDS analysis of impurities of the milling experiment

For higher magnification, scanning electron microscope (SEM), has been

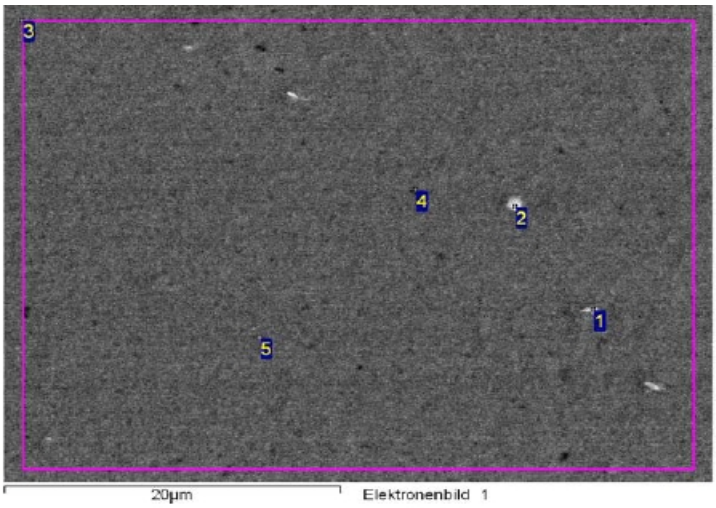

Spektrum	O	F	Al	Si	Ca	Cr	Fe	Summe
	in wt.%							
1	2.40	5.19	82.65	0.57	0.59	0.75	7.85	100.00
2	1.76		68.66	0.74	0.38		28.47	100.00
3	1.98	7.29	89.41	1.06	0.25			100.00
4	1.48	4.09	92.67	1.21	0.56			100.00
5		5.01	94.99					100.00

Figure 13: Material 4, detection of impurities

used. The chemical composition of the microstructural features was determined by energy dispersive spectrometer (EDS). By EDS analysis impurities were detected in the milled powder material containing the elements O, F, Al, Si, Ca, Cr, Fe and Ni (Figure 13, Figure 12).Fe and Cr rich impurities have their origin from wear of the milling equipment. Impurity of Ca can be caused by the cleaning process of the milling device. F contamination is caused by the HF - etching of the polished sample.

Impurity of Ni can be caused by remains at the milling equipment during a previous milling experiment.

3.3 Mechanical Testing

The mechanical behavior of the nano composites is probed by performing uniaxial compression and indentation. The results of these tests are presented in this section. Compression tests were performed at the Department of Mechanical Engineering, University Aveiro.

3.3.1 Compression Tests

A compression test is a method for determining the behavior of materials under a compressive load. The specimens are compressed, and deformation at various loads is recorded. Compressive stress and strain are calculated and plotted as a stress-strain diagram which is used to determine the elastic limit, proportional limit, yield point, yield strength and the compressive strength. Stress - strain diagrams have been constructed from data obtained in the compression test where its load is applied material 1 - 6, and continuous measurements of stress and strain are made simultaneously.

Compression tests with material 1 – 6 were performed using a Shimadzu AG-50 kN testing machine and the deformation was measured with a

Messphysik ME46 video-extensometer, Figure 14. The strain rate used in all tests was 2 x 10^{-3} s^{-1}. The lubricant Molykote was used to reduce friction with the loading plates in compression.

Figure 14: Compression Test Machine at University Aveiro

The test procedure involves placing the test specimen in the testing machine and applying compression until a maximum stress of about 970 - 990 MPa. Figure 15 shows test Material 3 before compression, and Figure 16 shows Material 3 after compression. 45 KN has been applied to each testing sample a circular cylinder with flat ends. The elongation measurement is used to calculate the engineering strain, ε, using the following equation:

$$\epsilon = \frac{\Delta L}{L_0} = \frac{L - L_o}{L_o} \quad (1)$$

where ΔL is the change in length, L_0 is the initial length, and L is the final length of the cylindrical material test sample. The force measurement is used to calculate the engineering stress, σ, using the following equation:

$$\sigma = \frac{F_n}{A}, \quad (2)$$

where F_n is the force normal to the cross-section A of the cylindrical specimen section.

Figure 15 shows Material 3, before testing:

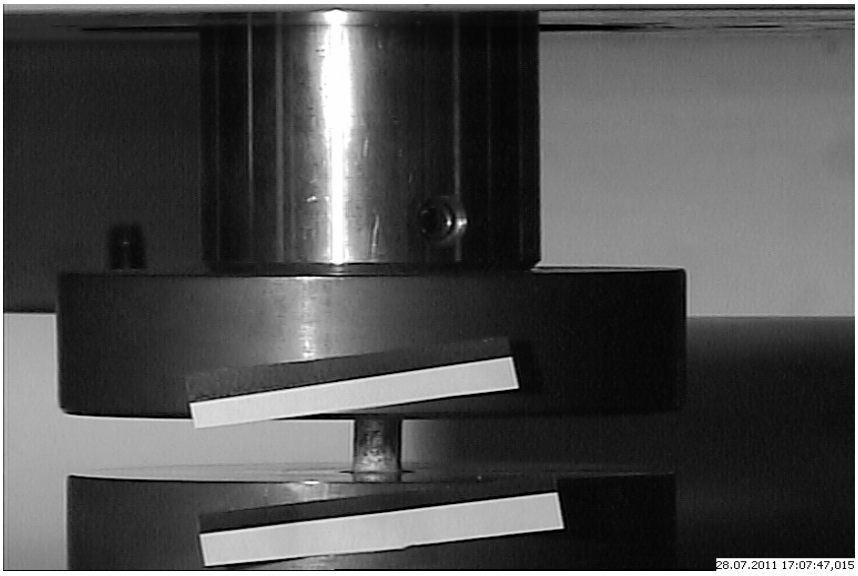

Figure 15: Material 3, before compression

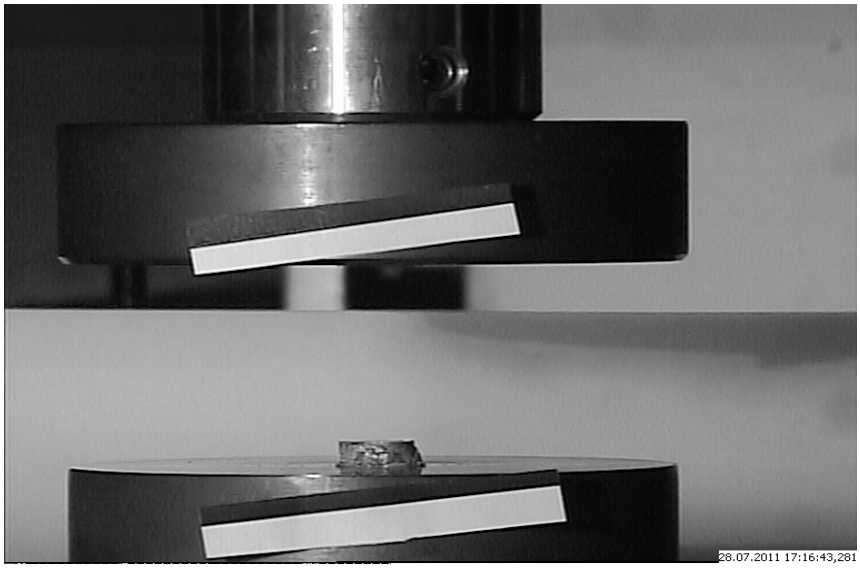

Figure 16: Material 3, after compression

Figure 16 shows Material 3, after testing:

Samples are deformed as depicted in Figure 17:

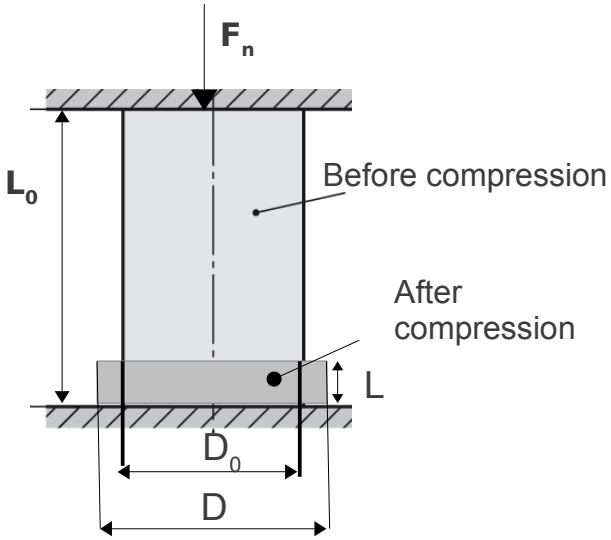

Figure 17: Sample before test performance

On compression, the specimen will shorten. The material will tend to spread in the lateral direction and hence increase the cross sectional area A as follows:

$$A = \frac{\pi * D^2}{4} \quad (3)$$

The results of the compression tests are shown in Table 3, in Appendix 7.5.

3.3.2 Indentation Tests

Indentation was performed to characterize the mechanical behavior at the nanoscale. The test was performed with a Berkovich tip. As well-known, the measured hardness varies with the indentation depth if indents are relatively shallow [18], and becomes insensitive to this parameter beyond a certain indentation depth.

In indentation small loads and tip sizes are used, so the indentation area may only be a few square micrometers or even nanometres. This presents problems in determining the hardness, as the contact area is not easily found. Atomic force microscopy or scanning electron microscopy techniques may be utilized to image the indentation, but can be quite cumbersome. Instead, an indenter with a geometry known to high precision, a Berkovich tip which has a three - sided pyramid geometry is employed. During the course of the instrumented indentation process, a record of the depth of penetration is made, and then the area of the indent is determined using the known geometry of the indentation tip. While indenting, various parameters such as load and depth of penetration can be measured. A record of these values plotted on a graph to create a load-displacement curve. These curves

can be used to extract mechanical properties of the material.

Indentation tests have been performed using a Nano Test 550 machine from Micromaterials Inc., UK, and a Berkovich tip. The indentation and retraction rates were equal and set at 27 °C. The tests are performed in load control and the displacement of the tip is measured with below 1 % error.

The Berkovich tip has the same projected area to depth ratio as a Vickers indentation as shown Figure 18.

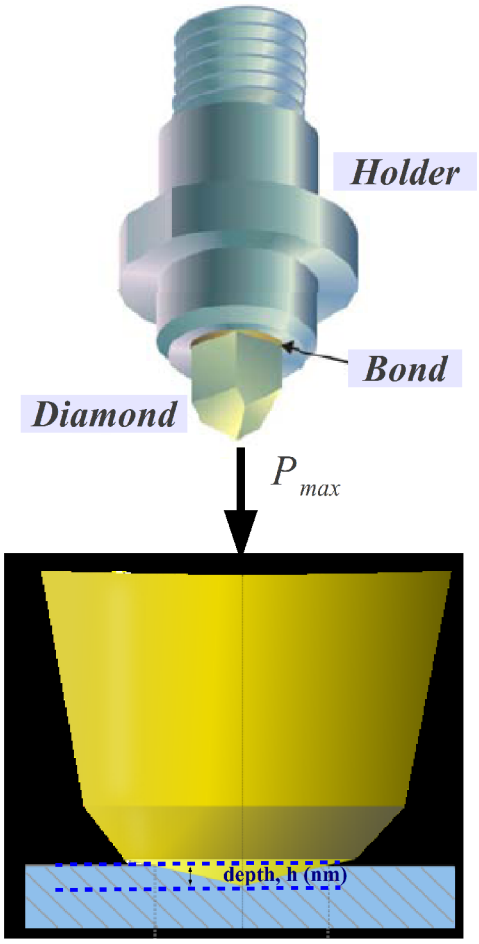

Figure 18: Berkovich nanoindentation tip (Retrieved from: Micro Star Technologies, www. microstartech.com).

$$H = \frac{P_{max}}{26{,}43 * h^2} \quad (4)$$

P_{max} is the maximum load, h is the penetration depth and H is the hardness.

The results of the hardness tests are shown in Table 4, in Appendix 7.5.

3.4 Transmission Electron Microscopy Investigations

The dislocation structure of the material before and after compression testing observed with a Hitachi H-9000 (300 kV) transmission electron microscope (TEM). The TEM samples were taken from the plane perpendicular to the cylindrical sample axis at the mid-thickness location of the specimen. The samples were mechanically polished on both surfaces and were electro polished using a double-jet thinner with a dilute solution of HNO_3 and methanol under 12 V tension at 20 °C. Figure 19 shows a TEM micrograph of material 3, containing 1 Vol. % SiC before (Figure 19a) and after (Figure 19b) the compression test. Most grains are equiaxed and of approximate size 100 nm. In addition, elongated grains, with the smaller dimension of approximately 50 nm and the larger dimension of about 500 nm were observed in some regions of the sample. For the samples tested in uniaxial compression the grains present a high and roughly uniform dislocation density.

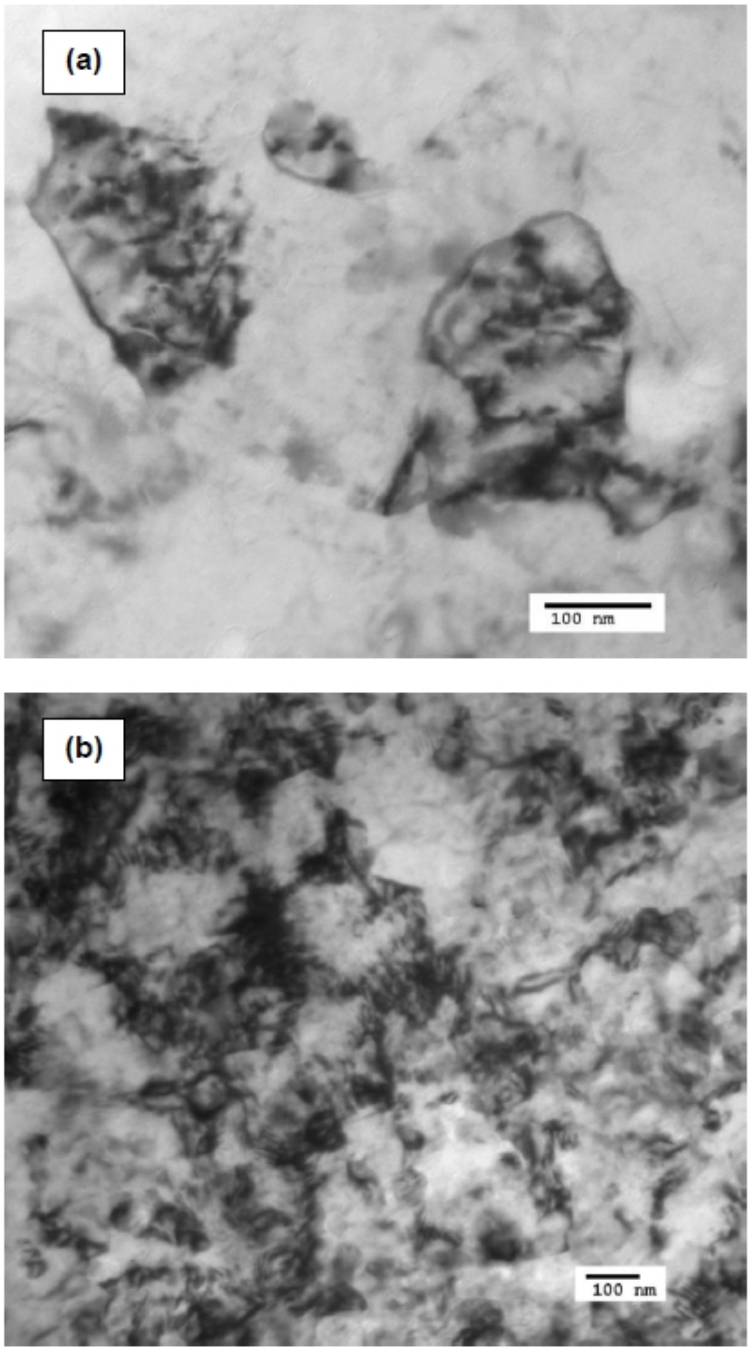

Figure 19: TEM micrographs of material 3 (a) after SPS processing and (b) after SPS processing and compression testing.

Figure 20 presents the dark field TEM image of the same sample showing well-defined SiC nanoparticles which are observed to be located predominantly at grain boundaries. An excellent distribution of SiC was also observed by fracturing one of these samples followed by performing scanning electron microscopy of the fracture surface. The SiC particles were identified visually and then their chemical composition was confirmed with EDS.

For further details analysis Scanning Transmission Electron Microscope (STEM) was applied in order to investigate the location of SiC nanoparticles in the aluminum matrix.

For these investigations material 3 after SPS processing containing 1

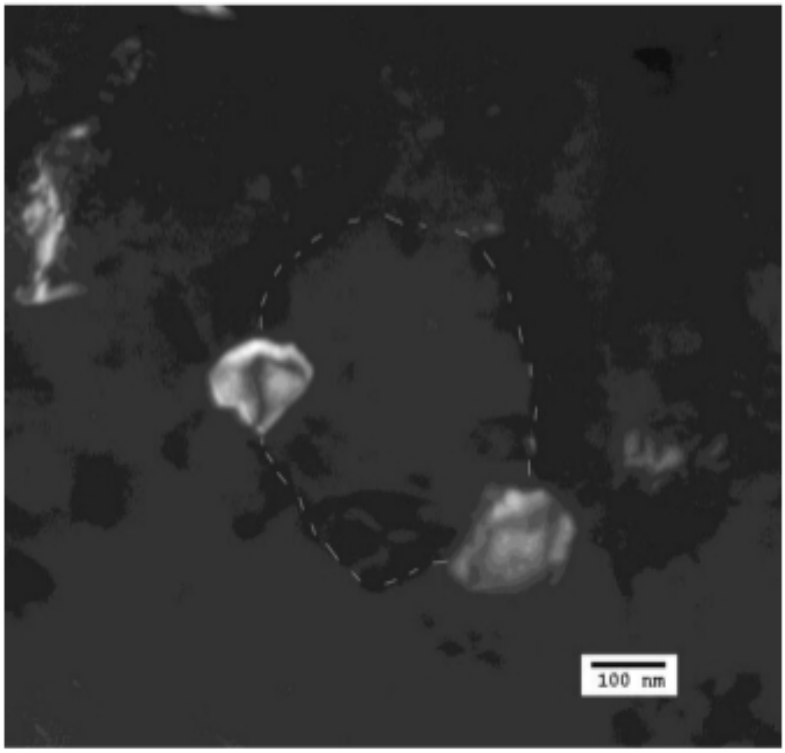

Figure 20: Dark field TEM micrographs of SiC nanoparticles located at grain boundaries (dashed line) in material 3

Vol. % SiC, was used. The samples were cut in two pieces. For STEM

analysis thin lamellae were prepared using the Focus Ion Beam (FIB) method. For this purpose the fracture surface of the specimen was polished and the FIB lamellae were extracted of this polished surface. Figure 21 shows location of the two extraction points whereas Figure 22 is a schematic presentation of the lamellae location in the as-received material.

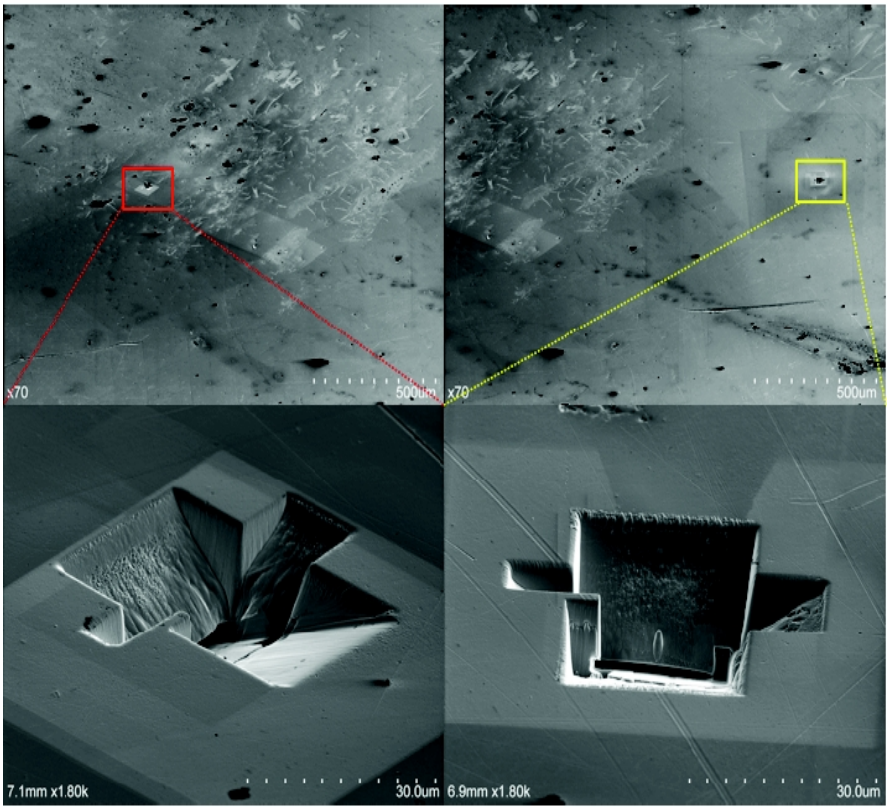

Figure 21: Material 3, location of 2 FIB lamellae extraction points on the polished fracture surface

Two lamellae were produced. While mounting a lamella to the electron microscope holder small tilting might have occurred, therefore the exact orientation of the microstructural features with regards to the sample rotation axis is not to be deduced form the images presented.

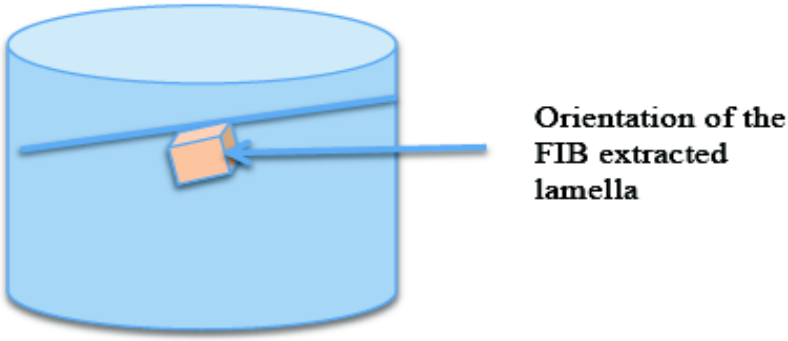

Figure 22: Lamellae location in the as-received sample

The results of the investigations for the first lamella are shown in Figure 23 and Figure 24.

In the Figure 23 elongated aluminum grains are shown. The longer axis of the grains is roughly oriented along the vertical axis of the as-

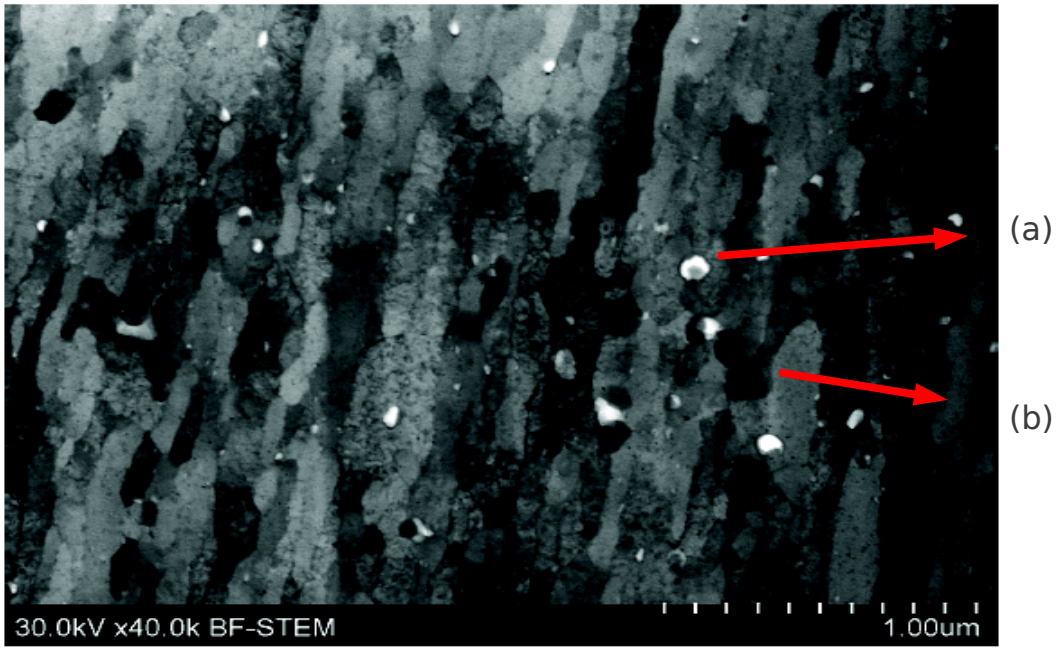

Figure 23: Microstructure of the first lamella as observed with STEM

(a) SiC particle, (b) elongated Al-grain

received material. The grain elongation may be due to electrical field assisted / augmented diffusion during sintering of the material in SPS.

The SiC nanoparticles are uniformly distributed in the matrix, no agglomeration of nanoparticles was observed.

A preferential location of the nano SiC particles at the matrix grain boundaries was observed.

At high magnification Figure 24 bright or dark dots are visible, depending on the contrast mode of the investigation. These dots are from the FIB preparation, re-deposits, mixture of the milled material tungsten and gallium used in FIB processing. Also tiny dark spots are also observed in Figure 24.

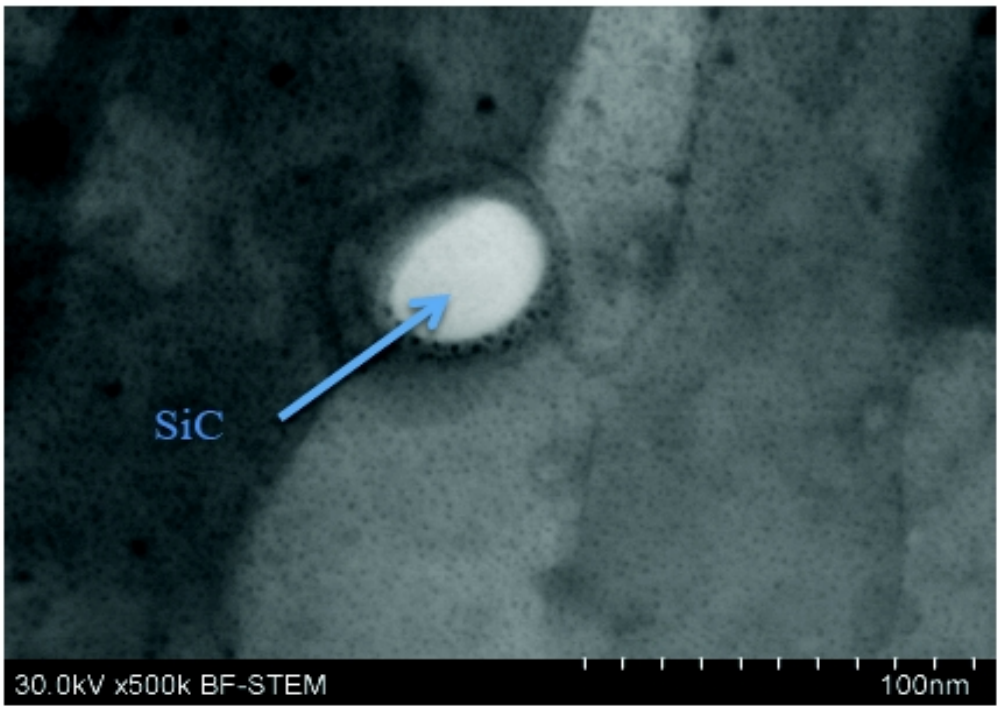

Figure 24: Microstructure of the first lamella as observed in transmitted electrons; through-thickness projection

These are radiation damages, introduced by the high-energy ions used for FIB milling. The EDS analyses shown that the main elements present in the sample were: Al, Si, C and O. Oxygen both from oxidation of elementary Al powder before milling or during SPS sintering as well as

surface polishing of the as-received sample for FIB processing. The EDS spectra show also presence of Fe, Cr and Ni . These particles are most probably debris of milling/mixing tools made of stainless steel.

Finally, all the EDS spectra show presence of Cu. This is related to material of sample holder and therefore copper should not be regarded as constituting element of the analyzed sample.

The lamella had sub areas with elongated and more equiaxed aluminum grains.

4. Results and Discussion

4.1 Microstructural Observations

The preferential distribution of ceramics particles at grain boundaries indicates that these do not act as obstacles to dislocations, as is generally the case in materials with larger grains. Hence, Orowan looping and dislocation pinning at fillers do not operate as hardening mechanisms in these materials. Nevertheless, the large difference between the thermal expansion of SiC and Al may lead to dislocation nucleation from the carbide particles upon temperature variation. The observation of the preferential location of particles at grain boundaries is opposite to the work reported in Poirier et al. 2010 [56], in which Al_2O_3 nanoparticles were seen to be located predominantly within the Al grains. Very few dislocations are visible in these samples. This is a common observation in nano crystalline materials and is attributed to the trapping effect of grain boundaries. Under deformation, the grain boundaries also play the role of dislocation sources, so the lack of dislocations does not imply a lack of dislocation activity during loading. The chemical composition of these materials was studied with EDS. The

main constituents are, of course, Al, Si and C. Traces of O were detected; its origin is thought to be related to the presence of oxides on the as-received Al particles. Occasionally, a flake of stainless steel resulting from the wear of milling balls or contained wall was detected.
When AlSiC nano composites are processed by the melt procedure, the flowing reaction was observed to take place at the filler-matrix interface in Saberi et al. 2009 [57]:

$$4Al + 3SiC = Al_4C_3 + 3Si \quad (5)$$

The presence of such phase was not detected in any of materials.
The interfaces are sharp and clean. This is due to the fact that the temperature reached during processing (both milling and SPS) is kept at low values. Perfect interfaces have been also observed for this system in Ye et al. 2005 [58], Cheng et al. 2008 [59], El-Eskandarany 1998 [20], Suryanarayana 2001 [60]. Generally, milling is reported to produce strong metallurgical bonds between reinforcements and the matrix in Suryanarayana 2001 [60]. A direct measurement of the interface strength in these samples is not possible. Carbon may be embedded in the Al matrix following the decomposition of the stearic acid during milling and at temperatures as high as 450 °C in Poirier et al. 2011 [61]. This leads to the formation of Al carbides which are not necessarily located close to the SiC fillers. This reaction renders the material heat treatable to some extent, with the hardness varying during heat treatment. On the other hand, it has been repeatedly observed in composites in which the matrix is a heat treatable Al alloy in Cheng et al. 2008, [59]. Parvin et al. 2008 [62] that precipitation becomes sluggish when the grains reach nanoscale dimensions. This is attributed to the fact that solute is preferentially trapped at grain boundaries and

therefore the net solute concentration in the grains is smaller than the nominal alloy value. The materials processed by powder metallurgy are not fully compacted and hence their density is smaller than that of material 1. The values do not depend on milling time, acid concentration or SiC content. The carbide concentration is small enough to have little effect on the overall composite density. The only exception is material 3HT250 which has a density smaller than materials 3 and 3HT150. The heat treatment did not affect the density of material 2, as the reported values of materials 2, 2HT150 and 2HT250 are within the experimental error (±0.02). The density of material 1 is within the experimental error to 2.7 g/cm³, which is the value expected for bulk aluminum see Table 2.

4.2 Mechanical Tests

4.2.1 Compression Tests

Figure 25 shows the stress-strain uniaxial compression curves corresponding to materials 1, 2 and 3. Material 1 has a yield stress of 37 MPa, as expected for pure Al with relatively large grains. The yield stress in tension is identical to that in compression. Material 2 has a yield stress of 276 MPa, 7.45 times larger than that of the reference material 1. This is due entirely to the reduction in grain size. The Hall-Petch effect in AA1050 was reported in Scharnweber et al. 2010 [63]. The effect is described by the equation:

$$\sigma_y[MPa] = 80 + 52\mathrm{d}^{-1/2}[\mu m] \quad (6)$$

where d is the grain size, which holds for d < 4 µm. For a grain size of

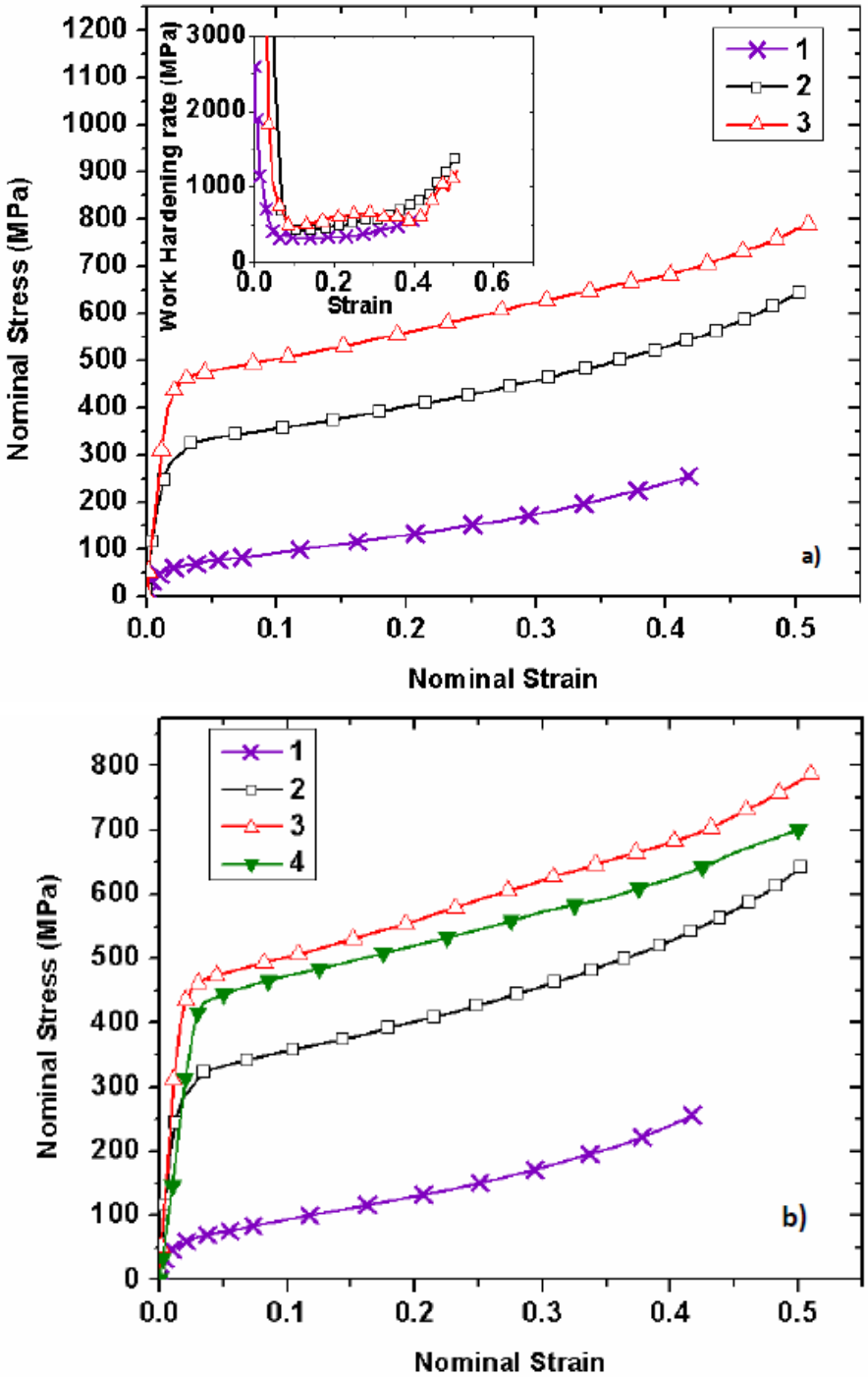

Figure 25: Nominal stress-strain curves from uniaxial compression tests of materials (a) 1, 2 and 3, and (b) 1, 2, 3 and 4

200 nm, this relation predicts σ_y = 196 MPa, while for d = 70 nm, it gives σ_y = 276 MPa like for material 2.

The addition of 1 Vol. % SiC leads to further increase of the flow stress. The curve corresponding to material 3 has a yield stress of 412 MPa, an increase by a factor of 11.1 relative to the reference material 1, and by a factor of 1.49 relative to material 2. It results that the main strengthening mechanism is associated with the presence of Al nanograins. The fact that SiC nanoparticles are located preferentially at grain boundaries indicates that precipitate/particle hardening does not operate, however the nanofillers slow down grain boundary sliding and migration. The additional strength gained by adding SiC nanoparticles is attributed to two mechanisms. On one hand, grain boundary pinning is expected to increase the flow stress since, given the small grain size of these samples, grain boundary sliding is expected to be important even at room temperature. On the other hand, the hard SiC particles are expected to be stress concentration sites and to act as sources of dislocations. The average wall-to-wall distance between nanoparticles at 1 Vol. % filling is 5.46 R, where R = 25 nm is the mean filler radius. This is equivalent to approximately 1-2 grain sizes. Hence, the confinement effect that the rigid fillers have on the plastic deformation of the matrix may also play a role in hardening. It is also interesting to observe in this context that the strain hardening rate is identical in all milled samples at given strain and is smaller in the un-milled material 1. The inset to Figure 25a) shows the strain hardening rate for all curves in the main figure. In alloys with precipitates and large grains the strain hardening rate is usually smaller than for the solid solution of same composition. Here we observe that the rate increases upon milling, and is insensitive to the presence of SiC particles. The increase is not surprising since the deformation mechanisms in materials 1 and 2 are quite different. We

interpret the insensitivity to the presence of SiC as a support of the conjecture made above that the nanoparticles, which are not embedded in the grains, do not interact with dislocations in the same way as in a precipitated alloys with micron-sized grains.

Similar conclusions have been reached in Poirier 2010 [56] while performing experiments with Al-10 Vol. % alumina nano composites prepared using a procedure similar to that applied here. In these experiments it was observed that the grain size reduction associated with milling has the largest effect. An increase of the yield stress by 3.46 times relative to the pure, unmilled Al, was observed, while the addition of alumina particles leads to a smaller increase a total of 4 times relative to the unmilled aluminum. Cryomilling Al-7.5 % Vol. Mg leads to an increase of the yield stress from 150 MPa to 575 MPa, a 3.83 times increase, and a reduction of the tensile strain at failure by 50 %, from 16 % to 8 %, reported in Han et al. 2003 [64]. A strong tension-compression asymmetry appears after milling and the strain hardening rate in tension is reduced. It is also interesting to compare with the corresponding micro-composite which has not been processed by milling in Cheng et al. 2008 [59]. When 12 Vol. % micron-sized SiC is embedded in large grains of diameter 50 nm, a 40 % increase of the yield stress was observed relative to the Al without SiC in Cheng et al. 2008, [59]. A 49 % increase is obtained in the tests, comparing materials 2 and 3, but this gain results upon the addition of only 1 % SiC.

Figure 25b) shows the effect of the SiC concentration.

The curves in Figure 25a) are shown together with that for material 4. The yield stress of material 4 is larger than that of material 2 by a factor of 1.46.

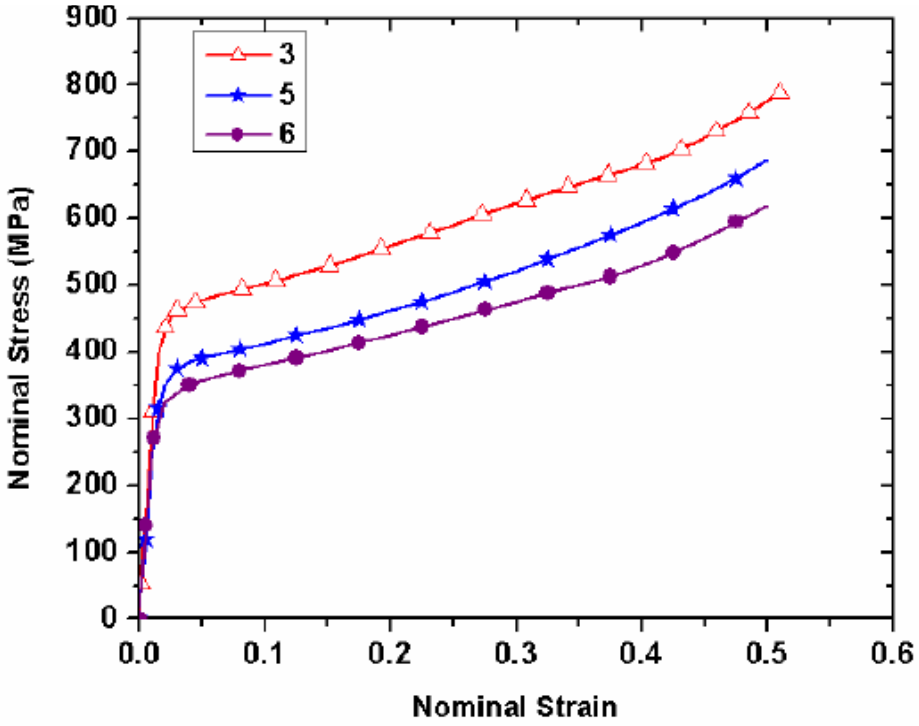

Figure 26: Nominal stress-strain curves from uniaxial compression tests of material 3, 5 and 6.

Figure 26 shows the response of process parameters for materials 5 and 6, compared to material 3. The yield stress of material 5, identical to material 3, except that its milling time was only 4.5 h, is 0.92 of the yield stress of material 3 and the aluminum grain size is around 150 - 200 nm. The SiC distribution is very good, as in all samples that have been processed by milling. The strain hardening rate is independent of the milling time.

Previous works on planetary ball milling have shown that the character of ball energy depends on the impacts, the size and number of balls in the vial. The same balls have been maintained in all mixtures done. Selection of the PCA, has been observed as process control agent, in this case was used stearic acid, and the milling time have a significant effect on the powder morphology. When stearic acid is used, micron sized composite powders are obtained. The hardness for the materials

milled with stearic acid is influenced by the mixing with the SiC nanoparticles and from the reaction of the stearic acid during milling. The hardness increases with the input energy. The influence of different processing parameters was studied for milling with the addition of 0.5 Wt. % of stearic acid as the process control agent. All parameters studied in this work as speed, time of milling, mass of balls and powders, have been assumed and experimented according the experience and studies already done in this area. A pronounced decrease in energy transfer from the balls to the powder is done with an increasing number of balls, when the milling is performed at low vial filling levels. Our experiments have been done always with the same balls and its amount, 100 g, and diameter, 10mm. Increasing the time milling, and using 1 Vol. % stearic acid, we observed that the material gets more homogeneous.

Stearic acid is added to the powder as a milling additive. It prevents the powder from sticking to the balls and the interior of the processing chamber. It has been reported that this addition helps reduce the size of the powder, speeding up the milling process. In these experiments it is observed that the yield stress increases upon increasing the acid concentration, when all other parameters are kept constant. This effect is demonstrated in Figure 26 by comparing the curves corresponding to materials 5 compared with the increase corresponding to material 3 relative to material 2, which is a factor of 1.49. The dependence of mechanical parameters on the SiC volume fraction is non-linear, as also observed in Poirier et al. 2010 [56].

4.2.2 Indentation Test

The variation of the hardness with the depth for material 3 is shown in the inset to Figure 27. This information was used to define the indentation depth for all subsequent tests at 1200 nm. The main Figure

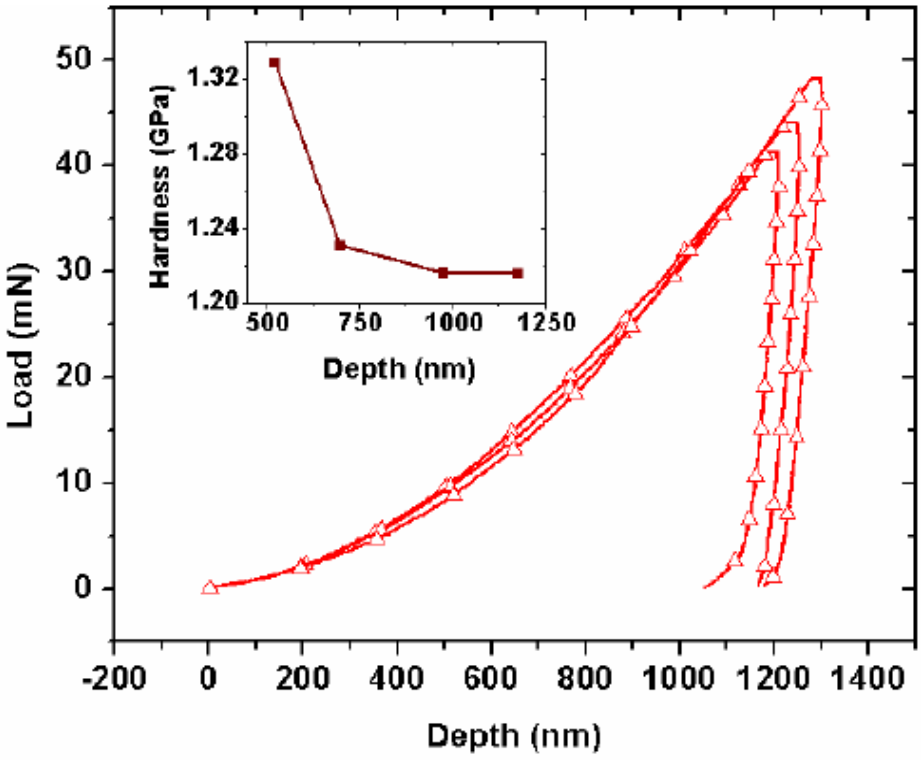

Figure 27: Load-displacement curves of three indentations in material 3 performed at different locations. The inset shows the variation of the hardness with the indentation depth

27 shows several force-displacement curves obtained by indenting material 3 at different sites.

The rather small variability observed in this figure indicates that the sample is homogeneous on this probing scale. Specifically, the probed volume of material in each of these tests is approximately 1 μm^3. This is in agreement with the discussion in the experimental chapter indicating good distribution of nanoparticles and sub-micron grain size.

Figure 28 shows load-displacement curves obtained for materials 1, 2, 3 and 4. This figure provides indentation data that complement the results shown in Figure 25b).

The conclusions and their implications are similar: a large increase in

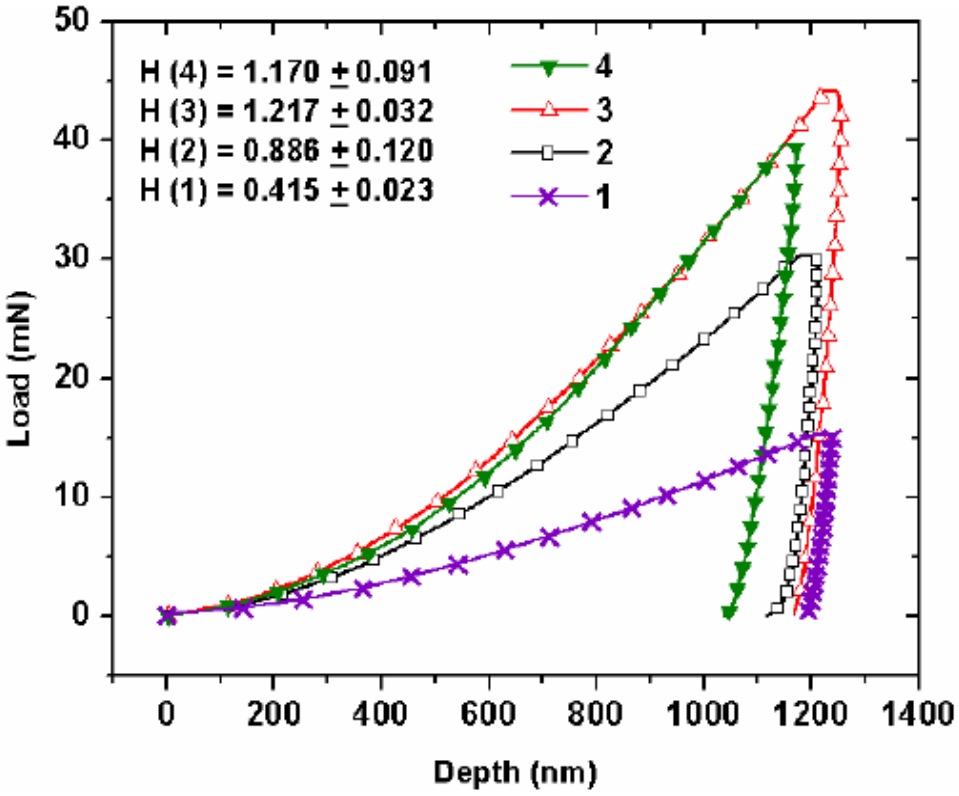

Figure 28: Load-displacement curves from indentations performed on materials 1, 2, 3, and 4

hardness results upon grain refinement (compare curves corresponding to materials 1, H = 0.41±0.023 GPa, and 2, H = 0.886±0.12 GPa), with a smaller increase being produced by the addition of SiC nanoparticles, comparing curves corresponding to materials 2, H = 0.886±0.12, and 3, H = 1.217±0.032 GPa.

Reducing the volume fraction of SiC leads to a small reduction of the hardness, material 4, H = 1.17±0.091 GPa. This represents increases relative to AA1050, material 1, of 2.16 times upon grain refinement, and of 2.75 times when 1 Vol. % SiC is added to the nanocrystalline

material. These increases are smaller than those computed based on the yield stress but the trends are identical.

A similar system was studied by Kamrani et al. [33] who evaluated the hardness of their samples as a function of SiC filling fraction using a classical micro-indenter. They report the ratio of the hardness of samples with 1 Vol. % SiC to the hardness of the nanocrystalline sample without SiC to be 1.25, which is comparable with the value of 1.37, material 3 relative to material 2, reported here. They indicate that the ratio of the hardness values increases to approximately 1.82 when the SiC concentration increases to 7 Vol. %. The fact that the SiC addition leads to a smaller increase of the hardness compared to the effect of milling is also reported in Parvin et al. 2008 [62], Fogagnolo et al. 2003 [65]. The numbers reported here can be also compared with the data presented by Parvin et al. 2008 [62] who studied AA6061-10 Vol. % SiC nano composites. They report the hardness of samples milled and then hot extruded, without SiC, as a function of milling time. The ratio between the hardness after 9 h of milling, maximum time of their study and the hardness of the unmilled AA6061 is 1.41, which may be compared with the effect of milling on AA1050: the ratio of the hardness of materials 2 and 1 is 2.16. As a side observation, it is interesting to note that the age hardening alloy AA6061 loses its aging capability upon milling in Parvin et al. 2008 [62].

Figure 29 shows the behavior of materials 3, 5 and 6. The figure

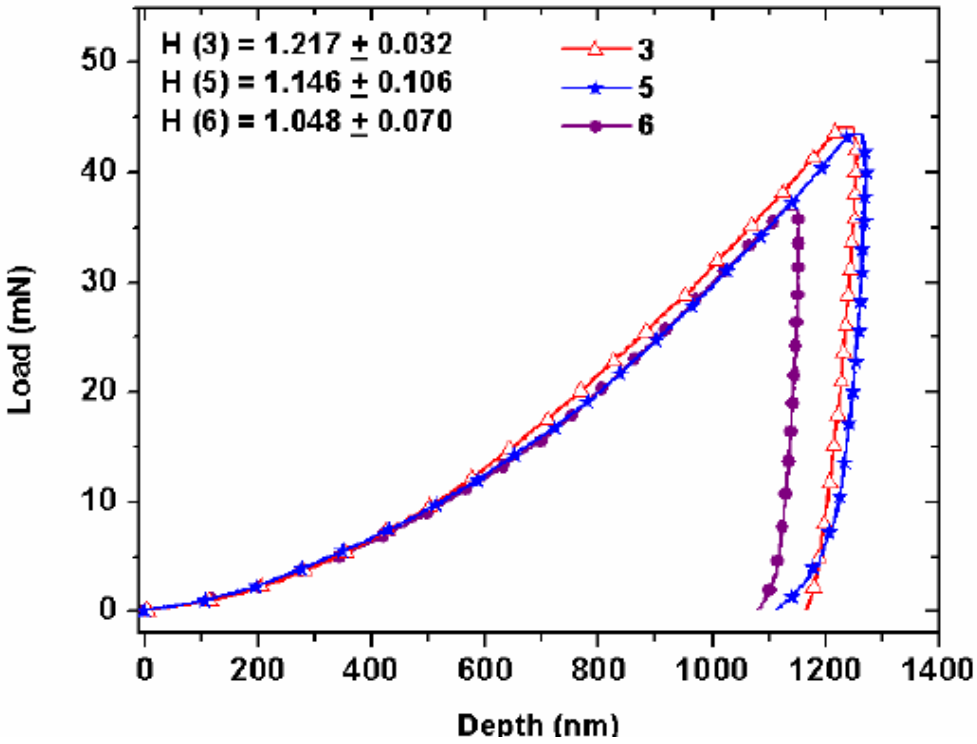

Figure 29: Load-displacement curves from nanoindentations performed on materials 3,5 and 6

parallels Figure 27 in which the uniaxial behavior of these samples is shown. The hardness of materials 3, 5 and 6 is H = 1.217±0.032 GPa, 1.146±0.106 GPa and 1.048±0.07 GPa, respectively. As before, their ranking in terms of hardness is identical to that established based on the yield stress, however, the ratios of yield stresses are not the same with those of the hardness values. A more pronounced increase of the yield stress relative to the increase of hardness upon the addition of nano-Al_2O_3 to Al was also reported in Kang and Chan 2004 [19].

4.3 Microstructural Stability to Annealing

The microstructural stability of these materials is essential in applications. In Al in particular, grain growth at ambient temperature is expected to take place leading to flow stress reduction and ductility improvement. To investigate this issue we selected the material leading to the highest yield stress, material 3, and its equivalent without SiC, material 2, and subjected them to accelerated aging by annealing at 150 ºC and at 250 ºC in separate experiments, for 2 h.

The samples were fully characterized by TEM, macroscopic uniaxial

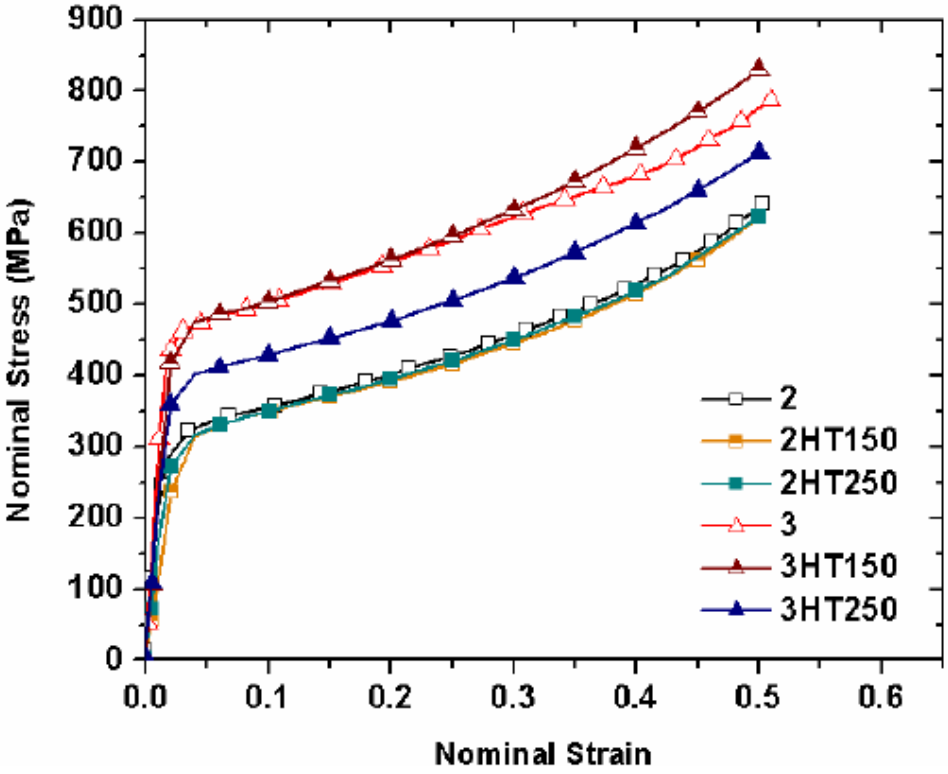

Figure 30: Nominal stress-strain curves from uniaxial compression tests of materials 2 and 3 before annealing and after heat treatment for 2 h at 150 °C and 250 °C

testing and indentation after each annealing sequence. The annealed materials 2 are denoted as 2HT150 and 2HT250, while the annealed materials 3 are labeled as 3HT150 and 3HT250.

Figure 30 shows the stress-strain curves of all samples before and after

annealing. The curves corresponding to the nanocrystalline material 2 without SiC before and after annealing overlap for both annealing sequences. The processed and 3HT150 curves overlap, however material 3 annealed at 250 °C loses some of its carrying capacity. Specifically, the yield stress drops from 412 MPa before annealing to 350 MPa after annealing at 250 °C.

To clarify the origin of these observations, TEM analysis has been performed on annealed materials both before and after deformation. The results indicate that in all materials with the same stress strain behavior before and after annealing there is no noticeable grain growth. However, the grain size of material 3, which was initially 150 nm, see Figure 19a) increases during annealing to approximately 200 nm, see

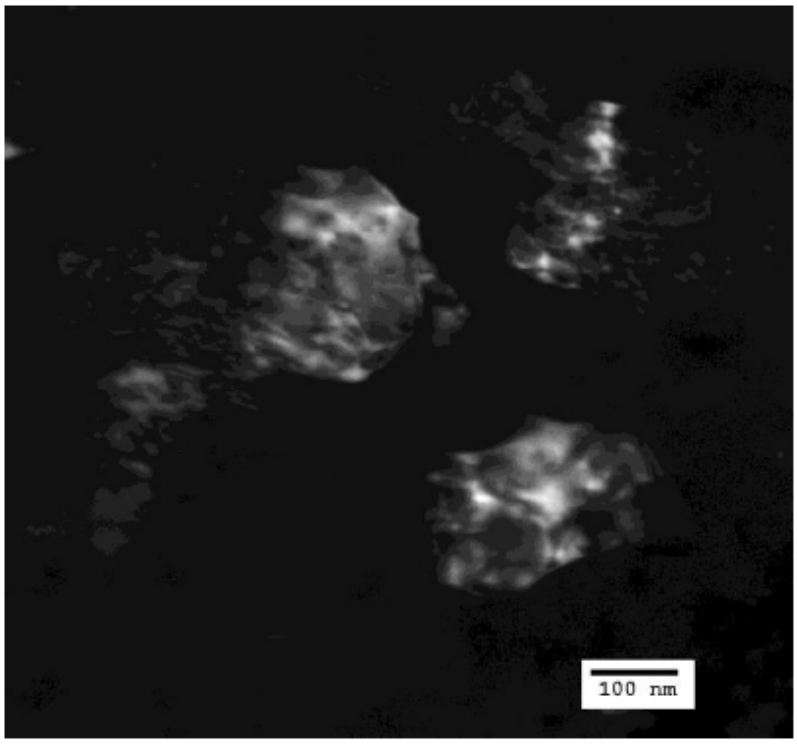

Figure 31: Dark field TEM micrographs of grains (white areas) of material 3 after annealing at 250 °C

Figure 31. The reduction of the yield stress observed for this sample is attributed to this change.

Similar conclusions regarding the stability of the microstructure of milled Al have been reported before. In Han et al. 2003 [64] it was shown that the annealing of cryomilled Al-7.5 Vol. % Mg at 450 °C for 2.5 h did not lead to significant grain growth and the yield stress was left essentially unchanged, although a slight improvement in ductility was observed. Relative insensitivity to annealing at 450 °C was also reported in Ye et al. 2005 [58] for a composite containing 10 Wt. % B_4C particles, nanocrystalline AA5083 and coarse grained AA5083 particles.

This 3-phase composite exhibited excellent yield stress (over 1 GPa) and excellent ductility. The stability of the milled microstructure is formally attributed to grain boundary pinning in Ye et al. 2005 [58], Zhou et al. 2001 [66], which, in our sample, should be enhanced by the presence of SiC particles at grain boundaries. However, a systematic study of the actual mechanism leading to microstructural stability in these materials with rough nanoscale features does not seem to be available in the literature.

Figure 32 shows indentation load-displacement curves for materials 2 and 3 in their heat treated and non-heat treated states. Local probing leads to conclusions similar to those described for Figure 30 All curves corresponding to material 2 overlap indicating that heat treatment has no effect on the microstructure of this material. Indeed no grain growth was detected in material 2 after annealing.

Indentation results for material 3 are rather similar before and after annealing. The reduction of yield stress observed after annealing at 250 °C in uniaxial testing is not reproduced when probing the material behavior at the nanoscale.

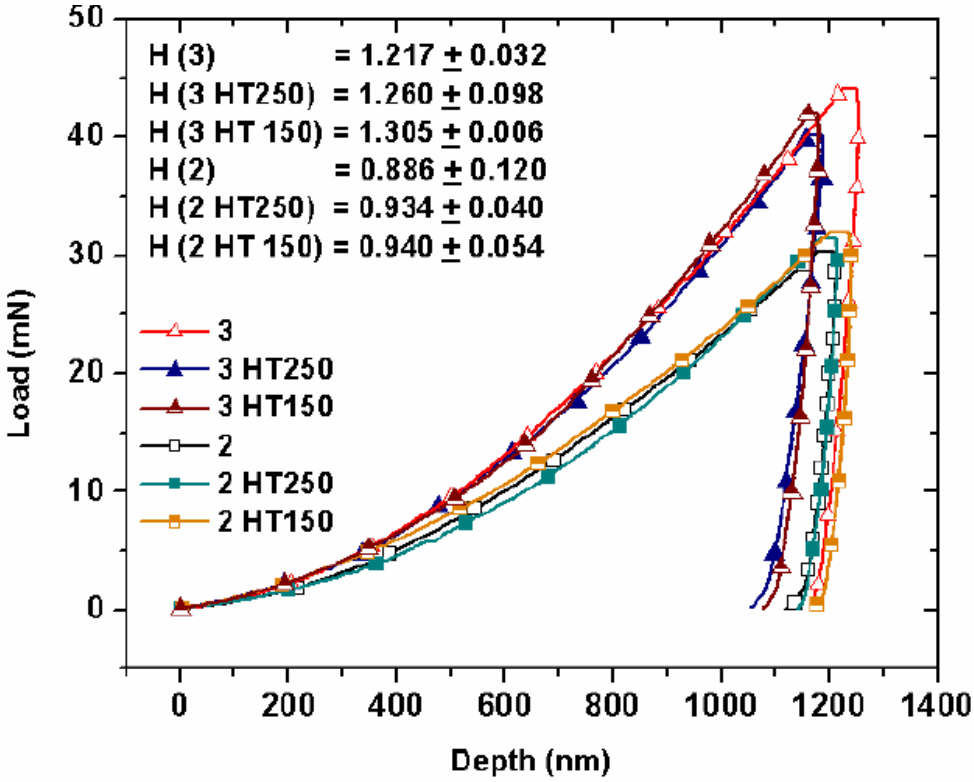

Figure 32: Load-displacement curves from indentation tests performed on materials 2 and 3 before annealing and after heat treatment for 2 h at 150 °C and 250 °C

4.4 Strengthening Mechanism

The description of plasticity in metal matrix composites have been analysed at different scales in several publications. The work of Saraev and Schmauder published in 2003 [67] proposed a simple model considering an elastic silicon carbide (SiC) inclusion and elastic-plastic aluminum (Al) matrix. The bonding between the inclusions and the matrix was assumed to be perfect. The plastic constitutive relations were taken in the Voce-type form with parameters fitted to the experimental data of Al 6061 alloy.

The model proposed by Chaboche et al. 2005 [68] was based on unit cell finite element analyses in the context of periodic homogenization

and delivered reference solutions for the overall stress–strain responses with various local constitutive behaviors. The particle size dependence for composite materials was studied by Liu and Hu 2005 [69] . In this scope, the authors proposed a new analytical micromechanical method in the framework of micropolar theory. In the work of Vena and co-workers in Vena et al. 2008) [70] a prescribed homogenized strain state is applied to a unit volume element of a metal–ceramic composite with proportional loading in which all components of the strain tensor are proportional to one scalar parameter.

The mechanical response of the material was modeled by considering a von Mises plasticity model for the metal phase and a Drucker–Prager associative elastic–plastic material model for the ceramic phase. The meso-mechanical constitutive model developed by Guo et. Al 2011 [71] proposes a nonlinear kinematic hardening rule to describe the ratcheting of metal matrix composites. With further assumption of spherical particles, the proposed meso-mechanical cyclic constitutive model was verified by comparing the predicted uniaxial ratcheting of SiCP/6061Al composites with corresponding experiments obtained at room temperature. A more physically oriented model was recently proposed by Azizi et al. 2011 [72]. In this work non-conventional boundary conditions are applied at material interfaces to model a constraint on plastic flow due to dislocation blocking. Unit cell calculations are carried out under generalized plane strain conditions. The plastic size effects due to dislocation pile-ups at interfaces were analyzed in the work of Okumura et al. 2011 [73].

It was shown that, strain hardening in elastic–plastic layers arises depending on thickness and stiffness of elastic layers; and the gap between slip planes in adjacent elastic–plastic layers. A key research work for understanding the plastic deformation in nanoscale metallic

multilayers was recently published by Zbib and co-workers 2011 [74]. The authors investigated the mechanical behavior of nanoscale metallic multilayered composites which is governed mainly by interface properties of coherent and/or incoherent interfaces, dislocation mechanisms in small volume, and dislocation–interface interaction, within a dislocation dynamics framework.

One important result in the context of the present work was the recent publication by Zhu and Lu 2012 [75], on modelling the plastic deformation of nanostructured metals with bimodal grain size distribution. The motivation for the model was a key experimental observation that nanograins or ultrafine grains contribute to high strength, while high ductility is attributed to coarse grains.

From the previous models and respective experimental data it is clear that the results obtained in the present work are unique essentially because the microstructure of the Al1050-SiC nano composite was tailored to have overall properties, very high yield stress and elongation. Simultaneously, the role of new microstructure-operative mechanisms during plastic deformation are emphasized. In fact, as the grain size is reduced, a transition is observed in the dominant strengthening mechanisms.

Figure 33 provides a schematic representation of this effect. In the case of micron-sized Al grains, the SiC particles are embedded in the grains and act as pinning sites for dislocations. The principal strengthening mechanism results from this interaction, Orowan looping.

In nanocrystalline Al, the flow stress is controlled by the Hall-Petch effect. As observed in this work, the added SiC particles segregate at grain boundaries and do not contribute to strengthening through the Orowan mechanism, rather pin the grain boundaries helping to stabilize the nanostructure of the material. Grain boundary sliding is expected to

be important in both nanocrystalline Al and AlSiC, although we do not present explicit proof for the operation of this mechanism at room temperature.

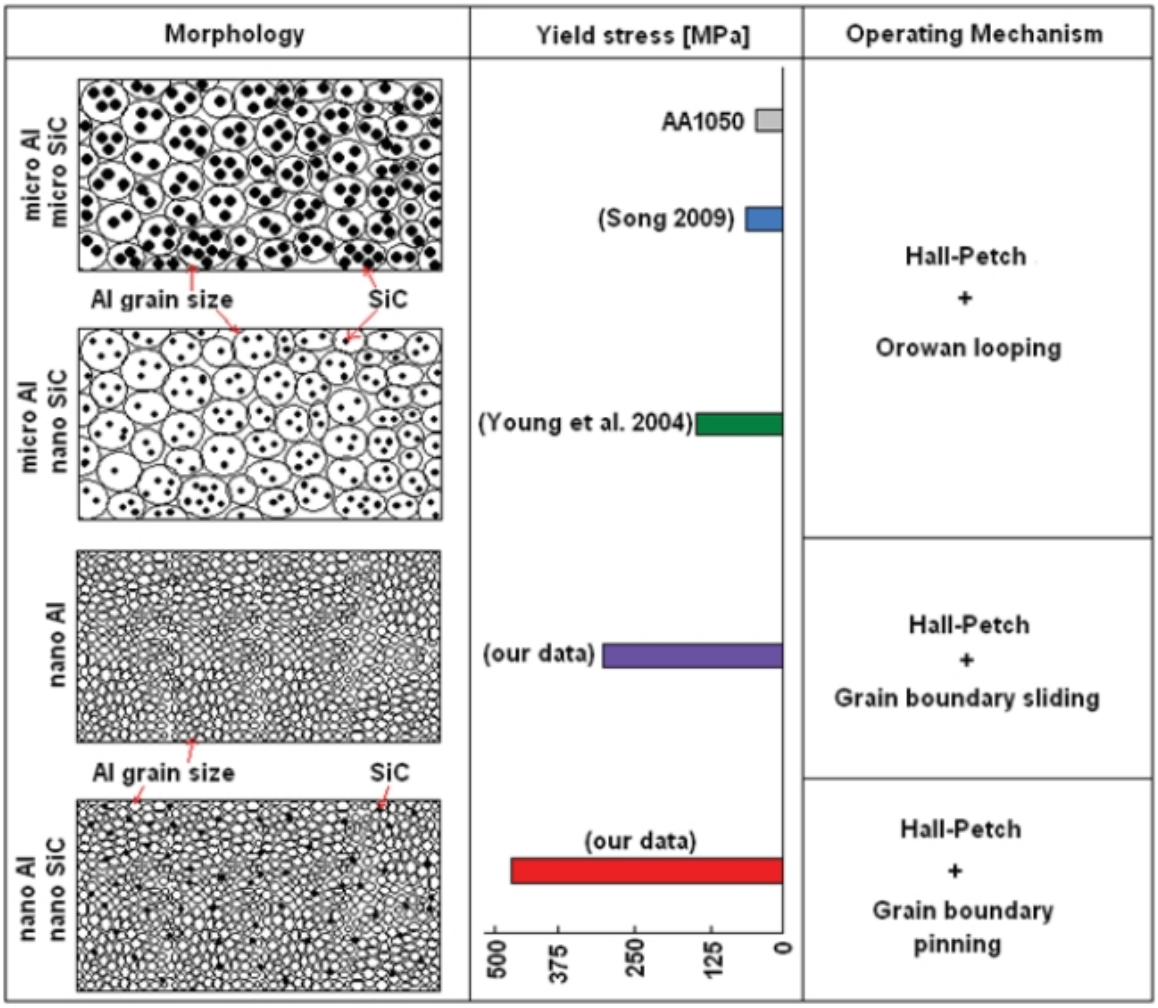

Figure 33: Schematic representation of microstructure transition mechanism from micro to nano Al-SiC composite

5. Conclusions

AlSiC nano composites were produced using a powder metallurgy technique and spark plasma sintering and their mechanical properties were studied on the macroscopic scale by uniaxial compression and at the nanoscale by indentation. The effect of process parameters, in particular that of milling time and concentration of stearic acid used, and of the concentration of SiC has been studied. The yield stress of the nano composite with optimal microstructure is more than one order of magnitude larger than that of the pure Al base material. This large increase is due primarily to the more than two orders of magnitude decrease of the grain size produced by milling. The addition of 1 Vol. % SiC accounts for 36 % of this increase. Increasing the stearic acid concentration leads to a measurable increase of the yield stress.

All these conclusions are confirmed when probing the material behavior locally, using indentation, although the measured hardness values are not always varying in proportion with the yield stress. A transition mechanism from micro to nano AlSiC composite is proposed for the understanding of the extraordinary mechanical properties, opening the doors for more sophisticated microstructure-based models.

6. Outlook

The strengthening effect of the dispersion of nano-SiC particles in pure aluminum, produced by ball milling of the powders and consolidation by Spark Plasma Sintering has been demonstrated and the related strengthening mechanism have been discussed. However, the successful application of the nano AlSiC composite, requires on the one hand an upscaling of manufacturing process parameters. On the other hand a component design related material property database, e.g. tensile test data, fatigue test data, creep test data as well as impact resistance test data are required.

7. Appendix

7.1 Abbreviations

CTE – Coefficient of Thermal Expansion

EDS – Energy Dispersive Spectrometer

FIB – Focus Ion Beam

ICE – Intercity – Express

PCA – Process Control Agent

HT – Heat Treatment

SEM – Scanning Electron Microscopy

SNCF - Société Nationale des Chemins de fer français

SPS – Spark Plasma Sintering

STEM – Scanning Transmission Electron Microscopy

TEM – Transmission Electron Microscopy

TGV – Train à grande vitesse

7.2 Chemical Symbols

Al – Aluminum

Al_4C_3 – Aluminum Carbide

Al_3Li – Aluminum Lithium

AlN – Aluminum Nitride

Al_2O_3 – Aluminum Oxide

B – Boron

BN – Boron Nitride

B_4C – Boron Carbide

Ca – Calcium

Cr – Chrome

CO_2 – Carbon Dioxide

Cu – Cooper

F – Fluorine

Fe – Iron

Ga – Gallium

HF – Hydrofluoric Acid

HNO_3 – Nitric Acid

Li – Lithium

Mg – Magnesium

MgO – Magnesium Oxide

Mn – Manganese

Ni – Nickel

O - Oxygen

Si - Silicium

SiC – Silicium Carbide

SiO_2 – Silicium Dioxide

Ti – Titanium

Y_2O_3 – Yttrium Oxide

Zn – Zinc

7.3 Physical Symbols

A – cross-section

b_{Mg} – burgers vector of magnesium

c – volume percent of alloy elements

d – grain diameter

D – final cross-section diameter of material compression test sample

D_0 – initial diameter of material compression test sample

d_T - particle diameter

ε – strain

F – force

F_n – force normal to cross-section

h – penetration depth

H – hardness

ky – Hall-Petch constant

L – final length of material compression test sample

L_0 – initial length of material compression test sample

P_{max} – maximum load

ρ - dislocation density

R_p – yield strength

V_f – volume fraction of particles

σ_0 - yield stress for dislocation movement (single crystal)

σ – stress

σ_y - yield stress

$\Delta\sigma_{GB}$ – grain boundary strengthening

$\Delta\sigma_{SH}$ – solid solution hardening

$\Delta\sigma_{PH}$ – precipitation / dispersion hardening

$\Delta\sigma_{WH}$ – cold work hardening

7.4 Aluminum Alloys

Alloy Group	Composition	Application
1000	99 - 99,99 Al	Chemical, building and food industry
2000	Al - Cu_4SiMg	Automotive, aeroplane, mechanical engineering structures
3000	Al – Mn	Like 1000 for higher strengths and chemical re-quirements
5000	Al – $Mg_{4,5}Mn_{0,7}$	Ship building structures, ship, industrial industry, vehicle structures
6000	Al- MgSiMn	Building structures vehicle parts electro engineering parts for improved strengths and corrosion resistance
7000	Al – Zn_5Mg_3Cu	Hight strengths applications (Aeronautic)

7.5 Tables Process Parameters and Investigation Results

Material	1	2	2HT150	2HT250	3	3HT150	2HT250	4	5	6
Density [g/cm³]	2.69	2.61	2.62	2.61	2.59	2.58	2.52	2.60	2.60	2.60

Table 1: Density values of all materials studied

Material No.	Al [g]	SiC [g]	SiC [Vol. %]	PCA [Wt. %]	Milling Parameters [h]	SPS Parameters	Heat Treatment
Material 1	AA1050	-	-	-	-	-	-
Material 2	10,000	-	-	1,0	9,0	450°C/5min/200 MPa	-
Material 2HT150	10,000	-	-	1,0	9,0		150°C /2h
Material 2HT250	10,000	-	-	1,0	9,0		250°C /2h
Material 3	9,880	0,118	1,0	1,0	13,5		-
Material 3HT150	9,880	0,118	1,0	1,0	13,5		150°C /2h
Material 3HT250	9,880	0,118	1,0	1,0	13,5		250°C /2h
Material 4	9,940	0,059	0,5	1,0	13,5		-
Material 5	9,880	0,118	1,0	1,0	4,5		-
Material 6	9,880	0,118	1,0	0,5	4,5		-

Table 2: Overview specimen materials

Material No.	**Specimen dimensions**				**Compression Parameters**	**Stress-strain analysis**		
	L_0 [mm]	**L [mm]**	**D_0 [mm]**	**D [mm]**	**Fn [kN]**	**R_p [MPa]**	**σMax [MPa]**	**εMax [-]**
Material 1	9,30	5,39	6,18	15,14	**45 at room temperature, v = 1 mm / min**	37	250	0,42
Material 2	9,30	4,65	7,57	9,46		276	640	0,50
Material 3	10,22	3,37	7,63	7,65		412	987	0,67
Material 4	10,18	2,85	7,69	7,68		403	971	0,72
Material 5	10,17	3,15	7,64	7,65		379	987	0,69
Material 6	10,27	2,98	7,62	7,65		345	987	0,71

Table 3: Overview compression test results

Material No.	Hardness, H [GPa]
Material 1	0.415+/-0.023
Material 2	0.886+/-0.120
Material 2HT150	0.940+/-0.054
Material 2HT250	0.934+/-0.040
Material 3	1.217+/-0.032
Material 3HT150	1.305+/-0.006
Material 3HT250	1.260+/-0.098
Material 4	1.170+/-0.091
Material 5	1.460+/-0.106
Material 6	1.048+/-0.070

Table 4: Overview of indentation results

8. Figures

Illustration Index

Figures

9. Bibliography

[1] Warren A.S.. "*Developments and Challenges for Aluminum – A Boeing Perspective* ". (2004) 28 : 24-31.

[2] European Aluminium Association. *“Sustainability of the European aluminium industry 2006”*. (2006) 467-236 : 1-48.

[3] Skillingberg M.. "*Aluminum Applications in the Rail Industry*". (2007) 1 : 1-5.

[4] Key to Metals AG. "*Aluminum Alloys in Military Vehicles and Equipment*". (2012) : .

[5] TU Wien. "*Applications - Brake rotors for German high speed train ICE-2*". (2007) : .

[6] Naser J., Ferkel H., Riehemann W.. *“Grain stabilisation of copper with nanoscaled Al2O3-powder”*. (1997) 234-236 : 470-473.

[7] Naser J., Riehemann W., Ferkel H.. *“Dispersion hardening of metals by nano scaled ceramic Powders”*. (1997) 234-236 : 467-469.

[8] Ferkel H.. *“Properties of copper reinforced by laser generated Al2O3 nanoparticles”*. (1999) 11 : 595 - 602.

[9] Ferkel H., Mordike B. L.. "*Magnesium strengthened by SiC nanoparticles*". (2001) 298 : 193 - 199.

[10] Witkin D., Han B. Q., Lavernia E. J.. "*Mechanical behavior of ultrafine-grained cryomilled Al 5083 at elevated temperature*". (2005) 14 : 519 - 527.

[11] Dai L.H., Ling Z., Bai Y.L.. "*Size-dependent inelastic behavior of particle reinforced metal-matrix composites*". (2001) 61 : 1057-1063.

[12] Mula S., Padhi P., Panigrahi S.C., Pabi S.K., Ghosh S.. "*On structure and mechanical properties of ultrasonically cast Al-2% Al2O3 nano composite*". (2009) 44 : 1154 - 1160.

[13] Goh C.S., Wei J., Lee L.C., Gupta M.. "*Properties and deformation behaviour of Mg-Y2O3 nano composites*". (2007) 55 : 5115 - 5121.

[14] Hassan F., Tan M. J., Gupta M.. "*High-temperature tensile properties of Mg/Al2O3 nano composite*". (2008) 486 : 5 6- 62.

[15] Scattergood R.O., Koch C.C., Murty K.L., Brenner D.. "*Strengthening mechanisms in nanocrystalline alloys*". (2008) 493 : 3 - 11.

[16] Tian B., Liu P., Song K., Li Y., Liu Y., Ren F., Su L.. "*Microstructure and properties at elevated temperature of a nano-Al2O3 particles dispersion-strengthened copper base composite*". (2006) 435-436 : 705 - 710.

[17] Hemanth J.. "*Development and property evaluation of aluminum alloy reinforced with nano-ZrO2 metal matrix composites (NMMCs)*". (2004) 507 : 110 - 113.

[18] Ramakrishnan N.. "*An analytical study on strengthening of particulate reinforced metal matrix composites*". (1996) 44 : 69 - 77.

[19] Kang Y.C., Chan S. L. I.. "*Grain stabilisation of copper with nanoscaled Al2O3-powder*". (2004) 85 : 438 - 443.

[20] El-Eskandarany M. S.. "*Mechanical Solid State Synthesizing of SiCp/Al Nano composite*". (1998) 279 : 263-271.

[21] Vojtech D., Verner J., Serak J., Simancik F., Balog M., Nagy J.. "*Properties of thermally stable PM Al-Cr based alloy*". (2007) 458 : 371 - 380.

[22] Hahn S.- I., Hwang S. J.. "*Estimate of the Hall-Petch and Orowan effects in the nanocrystalline Cu with Al2O3 dispersoid*". (2009) 483 : 207 - 208.

[23] Mohles V.. "*Orowan process controlled dislocation glide in materials containing incoherent particles*". (2001) 309-310 : 265 - 269.

[24] Mohles V., Fruhstorfer B.. "*Computer simulations of Orowan process controlled dislocation glide in particle arrangements of various Randomness*". (2002) 50 : 2503-2516.

[25] Zhang Z., Chen D. L.. "*Contribution of Orowan strengthening effect in particulate reinforced metal matrix nano composites*". (2008) 483-484 : 148-152.

[26] Vogt, Zhang, Li, Bonds, Browning, Lavernia and Schoenung. "*The absence of thermal expansion mismatch strengthening in nanostructured metal–matrix composites*". (2009) 61 : 1052 - 1055.

[27] Song H. W., Guo S. R., Hu Z.Q.. "*A coherent polycrystal model or the inverse Hall-Petch relation in nanocrystalline materials*". (1999) 11 : 203 - 210.

[28] Fedorov A. A., Gutkin M. Yu., Ovid'ko I. A.. "*Triple junction diffusion and plastic flow in fine-grained materials*". (2002) 47 : 51 - 55.

[29] Masumura R. A., Hazzledine P. M., Pande C. S.. "*Yield stress of fine grained materials*". (1998) 46 : 4527-4534.

[30] Benson D., Fu J. H.- H., Meyers M. A.. "*On the effect of grain size on yield stress: Extension into nanocrystalline domain*". (2001) 319-321 : 854 - 861.

[31] Smith C.. *"Grains, phases, and interactions: An interpretation of microstructure"*. (1948) 175 : 15-51.

[32] Gladman T.. "*The effect of second phase particles on grain growth*". (1966) 294 : 298 - 309.

[33] S. Kamrani, Z. Razavi Hesabi, R. Riedel, S. M. Seyed Reihani. *Synthesis and characterization of Al-SiC nanocomposites*. (article in press) : .

[34] Song X., Liu G., Gu N.. "*Influence of the second-phase particle size on grain growth based on computer simulation*". (1999) 270 : 178 - 182.

[35] Durisin, Durisinova K., Orolinova M., Saksl K.. "*Effect of the MgO particles on the nanocrystalline copper grain stability*". (2004) 58 : 3796 - 3801.

[36] Zhang Z., Chen D. L.. "*Consideration of Orowan strengthening effect in particulate reinforced metal matrix nanocomposites: A model for predicting their yield strength*". (2006) 54 : 1321-1326.

[37] Razavi Tousi D. L., Rahaei M. B., Abdi M. S., Sadrnezhaad S. K.. "*Stabilization of nanostructured materials using fine inert ceramic particles*". (2010) 36 : 793 - 796.

[38] Srinivasan D., Chattopadhyay K.. "*Hardness of high strength nanocomposite Al-XZr(X=Si,Cu,Ni) alloys*". (2004) 375-377 : 1228 - 1234.

[39] Srinivasan D., Corderman R., Subramanian P. R.. "*Strengthening mechanisms (via hardness analysis) in nanocrystalline NiCr with nanoscaled Y2O3 and Al2O3 dispersoids*". (2006) 416 : 211 - 218.

[40] Cao B., Joshib Sh. P., Ramesha K. T.. "*Strengthening mechanisms in cryomilled ultrafine-grained aluminum alloy at quasi-static and dynamic rates of loading*". (2009) 60 : 619 - 622.

[41] Tokita M.. "*Industrial applications of advanced spark plasma sintering*". (2006) 85 : 32-34.

[42] Amigo V., Ortiz J. L., Salvador M.D.. "*Microstructure and mechanical behavior of 6061 Al reinforced with silicon nitride particles, processed by powder metallurgy*". (2000) 42 : 383 - 388.

[43] Yang Y., Lan J., Li X.. "*Study on bulk aluminum matrix nano-composite fabricated by ultrasonic dispersion of nano-sized SiC particles in molten aluminum alloy*". (2004) 380 : 378 - 383.

[44] Lan J., Yang Y., Li X.. "*Microstructure and microhardness of SiC nanoparticles reinforced magnesium composites fabricated by ultrasonic method*". (2004) 386 : 284 - 290.

[45] Tang F., Hagiwara M., Schoenung J.M.. "*Microstructure and tensile properties of bulk nanostructured Al-5083/SiCp composites prepared by cryomilling*". (2005) 407 : 306-314.

[46] Nygren M. , Shen Z.. "*Novel assemblies via Spark Plasma Sintering*". (2004) 69 : 211-218.

[47] Kessel H.U., Hennicke J., Schmidt J., Weißgärber T., Kieback B., Herrmann M., Räthel J. . "*Feldaktiviertes Sintern,* "*FAST*". (2006) : 201-237.

[48] Hulbert D. M., Anders, Dudina, Andersson, Jiang, Unuvar, Anselmi-Tambu. "*The absence of plasma in `spark plasma sintering*". (2008) 104 : 033305-1 – 7.

[49] Ryu J.R. , Moon K.I., Lee K.S.. "*Microstructure and mechanical properties of nonocrystelline Al-Ti alloys consolidated by plasma activated sintering*". (2000) 296 : 157-165.

[50] Ohashi O., Xie G.. *intering of aluminium alloy powders using pulse electric current sintering process*. (2008) : 680-685.

[51] Murakoshi Y., Sano T., Diewwanit I., Nakayama Y., Miyamoto S.. *Effect of extrusion on aluminium-lithium alloy composites sintered by SPS process*. (2001) 1 : 29-37.

[52] Nagae T., Yokota M., Nose M., Tomida S., Otera K., Kamiya T., Saji S.. *Microstructure and mechanical properties of gas atomized aluminium alloy powder compact densified by pulsed current pressure sintering process*. (2002) 43, no 3 : 537-543.

[53] Hummert K. , Schattevoy R.. *Anwendungen für PM-Aluminium – Höchstleistung bei niedriger, aber voller Dichte*. (2007) : 229-245.

[54] Zadra M., Casari F., Girardini L., Molinari A. . *Spark plasma sintering of pure aluminium powder: mechanical properties and fracture analysis*. (2007) 50 : 40-45.

[55] Schubert Th. , Schmidt J., Weissgärber T., Kieback B. . "*Microstructure and Mechanical Properties of an Al-Si Alloy Consolidated by Spark Plasma Sintering*". (2010) : .

[56] Poirier D., Drew R.A.L., Trudeau M.L., Gauvin R.. "*Fabrication and properties of mechanicallymilled alumina/aluminum nanocomposites*". (2010) 7605 : 527.

[57] Saberi Y., Zebarjad S.M., Akbari G.H.. "*On the role of nano-size SiC on lattice strain and grain size of Al/SiC nanocomposite*". (2009) : 484, 637.

[58] Ye J., Han B.Q., Lee Z., Ahn B., Nutt S.R., Schoenung J.M.. "*A tri-modal aluminum based composite with super-high strength*". (2005) 53 : 481.

[59] Cheng N.P., Zeng S.M., Liu Z.Y.. "*Preparation, microstructures and deformation behavior ofSiCP/6066Al composites produced by PM route*". (2008) 27 : 202.

[60] Suryanarayana C.. "*Mechanical alloying and milling*". (2001) 46 : 1.

[61] Poirier D., Legoux J.G., Drew R.A.L., Gauvin R.. "*Consolidation of Al2O3/Al NanocompositePowder by Cold Spray*". (2011) 20 : 275.

[62] Parvin N., Assadifard R., Safarzadeh P., Sheibani S., Marashi P.. "*Preparation and mechanical properties of SiC-reinforced Al6061 composite by mechanical alloying*". (2008) 492 : 134.

[63] Scharnweber J., Skrotzki W., et al.. "*Texture, microstructure, mechanical properties of ultrafine grained aluminum produced by accumulative roll bonding*". (2010) 12 : 989.

[64] Han B.Q., LeeZ., Nutt S.R., Lavernia E.J., Mohamed F.A.. "*Mechanical properties of an ultra fine grained Al-7.5 pct Mg alloy*". (2003) 34 : 603.

[65] Fogagnolo J.B., Velasco F., Robert M.H., Torralba J.M.. "*Effect of mechanical alloying on the morphology, microstructure and properties of aluminium matrix composite powders*". (2003) 342 : 131.

[66] Zhou F., Lee J.,Lavernia E.J.. "*Grain growth kinetics of a mechanically milled nanocrystalline Al*". (2001) 44 : 2013.

[67] Saraev D., Schmauder S.. "*Finite element modelling of Al/SiCp metal matrix composites with particles aligned in stripes a 2D–3D comparison*". (2003) 19 : 733–747.

[68] Chaboche J.L., Kanoute P., Roos A.. "*On the capabilities of mean-field approaches for the description of plasticity in metal matrix composites*". (2005) 21 : 1409–1434.

[69] Liu X., Hu G.. "*A continuum micro mechanical theory of overall plasticity for particulate composites including particle size effect*". (2005) 21 : 777–799.

[70] Vena P., Gastaldi D., Contro R.. "*Determination of the effective elastic–plastic response of metal–ceramic composites*". (2008) 24 : 483–508.

[71] Guo S, Kang G., Zhang J.. "*Meso-mechanical constitutive model for ratchetting of particle reinforced metal matrix composites*". (2011) 27 : 1896–1915.

[72] Azizi R., Niordson, Brian C.F., Legarth N.. "*Size-effects on yield surfaces for micro reinforced composites*". (2011) 27 : 1817–1832.

[73] Okumura D., Nobutada Ohno N., Yamaguchi K.. "*Plastic size effect analysis of lamellar composites using a discrete dislocation plasticity approach*". (2011) 27 : 2040–2055.

[74] Zbib H.M., Cory T., Verman O, Firas Akasheh F., Bahr D.. "*Analysis of plastic deformation innanoscale metallic multilayers with coherent and incoherent interfaces*". (2011) 27 : 1618–1639.

[75] Zhu L., Lu J.. "*Modelling the plastic deformation of nanostructured metals with bimodal grain size distribution*". (2012) 30-31 : 166–184.